From the Medizinische Klinik and Poliklinik IV
Campus Innenstadt
at the Ludwig-Maximilians-University of Munich
Director: Prof. Dr. med. Martin Reincke

The Qualitative Assessment of Biodegradable Coronary Stents with the Use of Intravascular Ultrasound, Optical Coherence Tomography and Histology

A Dissertation
Submitted for the Degree of Medicine
At the Faculty of Medicine
Ludwig-Maximilians-University
in Munich

Written by
Burcu Gül

From
Izmit, Turkey

2014

Mit Genehmigung der Medizinischen Fakultät
der Universität München

Berichterstatter:	Priv. Doz. Dr. Johannes Rieber
Mitberichterstatter:	Priv. Doz. Dr. med. Rainer Kozlik-Feldmann Prof. Dr. med Michael Näbauer
Dekan:	Prof. Dr. med. Dr. h.c. M. Reiser, FACR, FRCR
Tag der mündlichen Prüfung:	10.04.2014

For

Mükü, Burçin and My Parents

Table of Contents

Introduction

Why Biodegradable Stents?

Cardiovascular disease is still the leading cause of death in industrialized countries and is expected to become so in emerging countries by 2020[53]; chronic stable angina is its most common symptom[52].

Myocardial revascularization, or the restoration of adequate blood flow, plays a key role in the management of chronic stable angina. There are two procedures currently available for myocardial revascularization: coronary artery bypass graft (CABG) and percutaneous transluminal coronary angioplasty (PTCA). CABG is a surgical treatment performed on obstructed coronary arteries by grafting healthy vessels in order to bypass a blockage. The second procedure, PTCA, was introduced years later as a less invasive alternative to CABG; after placing a guiding catheter through the femoral, brachial or radial artery at the origin of the coronary artery, a balloon-tipped catheter is introduced into the coronary artery and inflated in order to expand the coronary artery wall at the site of the blockage, restoring normal blood flow.

PTCA is now the most popular treatment, though CABG has been the treatment of the choice for patients with certain types of indications[20]. Advantages of PTCA include being less invasive, more cost effective[34], having shorter recovery times, and its feasibility in acute myocardial infarction (MI) and high-risk coronary artery disease (CAD) patients. Comparisons of both methods in long-term outcomes shows that PTCA requires more repeat target vessel revascularizations (TVRs) due to the high number of acute vessel closures caused by coronary artery dissection, elastic recoil and restenosis[14], which all occur as a result of vascular tissue injury caused by angioplasty. In order to overcome this limitation, bare metal stents were introduced.

The advent of coronary stents (tubular wire mesh for intravascular mechanical support) has led to a new era in interventional cardiology. By implanting bare metal stents (BMS), all three limitations of PTCA – coronary artery dissection, elastic recoil and negative remodeling – are prevented[83]. It turned out, however, that implantation of bare metal stents brought some other major drawbacks with it: stent thrombosis and in-stent restenosis. Stent thrombosis is defined as a clot formation within the tubular

meshwork and can be effectively prevented through administration of dual antiplatelet therapy with ticlopidine and aspirin[11, 50, 30]. In-stent restenosis, on the other hand, is a result of deep focal vascular injury caused by stent struts, followed by excessive tissue proliferation[38]. There have been a number of different strategies developed to overcome this drawback.

The first and most effective strategy developed to overcome in-stent restenosis was brachytherapy (β and γ radiation delivered intracoronary to inhibit cell proliferation). This, however, led to stent thrombosis due to the failure of vascular tissue healing, and further restenosis at the stent edges caused by the proliferative effect of low dose radiation[4]. It wasn't until the invention of drug-eluting stents (DES) that interventional cardiology witnessed another breakthrough; and this novel innovation reduced in-stent stenosis rates drastically[36].

DES are essentially BMS coated with either anti-proliferative (eg. Paclitaxel) or immune modulating drugs (eg. Sirolimus substances) used to inhibit the biological processes responsible for in-stent stenosis. This technology has its own disadvantages: late malapposition, hypersensitivity reaction, chronic inflammation, elimination of vasomotion, and late stent thrombosis (after 1 year)[4, 41, 55, 36]. Another downside of DES, like all permanent stents, is that they are not compatible with computed tomography (CT) or magnetic resonance imaging (MRI) and to some extent preclude future surgical revascularization.

To overcome the inherent limitations of permanent stents (in-stent stenosis, late thrombosis and elimination of vasomotion), the medical industry has been investing heavily in new technologies. Based on data from studies employing intravascular ultrasound (IVUS), stent scaffolding for the prevention of restenosis is required to last for 6 months[63]. Therefore the ideal stent would fulfill its mission and step away[12] through biodegradation. These so-called biodegradable stents should be biocompatible (able to perform with an appropriate host response in a specific application)[64], as must be the product of their degradation, and they must provide proper scaffolding, radial force and endurance.

The first biodegradable stent was introduced by Stack et al. in 1988 using a polymer of poly-L-lactide (PLLA)[75]. Unfortunately, histopathological studies showed that implantation of these stents resulted in significant inflammatory responses and

neointimal proliferation with extensive cell infiltration, suggesting that PLLA was not completely biocompatible. In addition, there was also evidence of medial necrosis and pseudoaneurysm formation[79]. In 2001, an experiment with New Zealand white rabbits showed that biodegradable iron stents could be applied safely without significant obstruction of the stented vessel caused by inflammation, neointimal proliferation, or thrombotic events[60], though further clinical data is needed.

In the years following, Heublein et al. introduced biodegradable magnesium stents[33], a type of absorbable metals stent (AMS), which have since become an area of interest for numerous studies[16, 59, 5, 80, 23, 24]. Biodegradable magnesium stents have revealed both reduced intimal proliferation and larger minimum lumen diameters than BMS[24]. Later, Erbel et al. showed the feasibility and safety of biodegradable magnesium stents[23].

This brings us to the present day; before biodegradable magnesium stents can be introduced as a standard method for the treatment of coronary artery disease (CAD), more research is required to better understand the degradation kinetics and mechanical stability of these stents. It is also necessary to study the neointimal formation, inflammatory response of vessel walls to stenting and endothelialization of the stent struts. In order to accomplish these studies, however, the biodegradable magnesium stents must provide adequate opacity for visualization – wherein lies the challenge. It is not possible to visualize magnesium stents with coronary angiography, computed tomography (CT) or magnetic resonance imaging (MRI). Newer imaging modalities such as optical coherence tomography (OCT) and intravascular ultrasound (IVUS) have been proposed to exploit the ability of magnesium and its degradation products to reflect both light and sound[23, 61] in order to visualize their degradation.

The purpose of this research was to compare IVUS and OCT as in-vivo visualization techniques to capture the degradation progress and endothelialization of stent struts, and vessel geometry. To validate the results acquired with IVUS and OCT, histology was employed as an ex-vivo technique. And finally in order to capture the degradation process and kinetics at a cellular level, an alternative technique to the immersion and electrochemical test (the standard test for degradation studies), titan yellow staining, was also investigated.

IVUS (Intravascular Ultrasound)

IVUS is a catheter-based visualization technique that provides cross-sectional imaging of coronary vessels. A transducer is positioned at the end of the IVUS catheter. There are two different types of the IVUS transducer available: a mechanical transducer (a single transducer rotates with fixed array system on a drive shaft) and electronically switched multi-element array system. The array system contains of piezoelectric crystalline material that contract and expand to create sound waves when electrically stimulated[49]. Ultrasound images are produced by passing a current through these crystals. This in-vivo visualization technique uses a rotating ultrasound probe attached to the tip of a specially designed catheter to emit ultrasound perpendicular to the vessel walls (for a range of frequency between 20 and 40 MHz, the typical image resolution is 150-250 μm). Two factors are essential for the image quality: spatial resolution and contrast resolution. While spatial resolution describes the discrimination of small objects within the image, contrast resolution is the distribution of the gray scale of the reflected signal[49]. On an IVUS image a healthy vessel wall is displayed two layered: intima and media are displayed as one single echolucent intima-media complex because those two layers cannot be differentiate well in a 150 μm - 250 μm resolution. Adventitia is displayed as a single echogenic layer[74, 56].

IVUS enables exact assessment of vessel wall morphology and vessel geometry with low intra- and inter-observer variability[65]. It is considered superior to coronary angiography because it can detect areas of positive remodeling (increases in external elastic membrane (EEL)), which is of interest because an increase in EEL may be indicative of over-compensation from increasing plaque areas associated with high-risk of plaque rupture[58, 57].

One disadvantage of IVUS is its low accuracy in imaging particular areas, such as behind stent struts, due to acoustic shadowing and artifacts resulting from different impedance between the vessel wall and stent strut. Another is that its use in the assessment of neointima formation is also limited due to its relatively low axial-resolution (50μm)[21].

Despite these disadvantages, during the past decade IVUS has proved to be the standard of reference for qualitative assessment of coronary vessels due to its high

accuracy[26, 29, 47]. In particular, IVUS has helped determine the mechanism of in-stent stenosis[73] and plaque characteristics (concentric, eccentric, calcified)[25]. Finally, IVUS has also been instrumental in the visualization of biodegradable stents and in quantifying stent parameters for the qualitative assessment of its degradation process[16, 22, 23, 24, 33].

OCT (Optical Coherence Tomography)

OCT is an in-vivo infrared light-based imaging modality that relies on the use of interferometry - a technique used to measure light velocity. OCT utilizes an infrared light source (1300±50 nm wavelength) that is sent through a fiber optic and then split in to two arms: a sample arm and a reference arm. The sample arm reflects the transmitted light rotated through 360° in the vessel to provide a two-dimensional image. The interferometer combines the light returning from the sample arm with that of the reference arm in order to create an interference pattern containing information about the intensity of the optical back-scattering, displayed as a (false) color or gray scale image. Thus, OCT provides a two-dimensional (2D) cross-sectional real-time image. Both the bandwidth of the employed infrared light and the wave velocity are higher than in medical ultrasound and its typical resolution is 10microns[8], meaning it can provide in-situ images of tissues at near histologic resolution.

In the early 1990s, OCT was first applied in the field of ophthalmology[37]. Its subsequent vascular applications in the mid-‘90s demonstrated the potential of the technique to identify clinically relevant coronary artery morphology with a level of resolution higher than any other clinically available diagnostic imaging modality[8, 39]. A healthy non- atherosclerotic vessel presents three layers on OCT. Intima is displayed as bright and high reflective band. Media has a weak signal intensity, while adventitia has a stronger signal intensity[7]. Thanks to this high-resolution tomographic intra-arterial imaging, OCT has proven to be accurate in characterizing atheromatous plaque in a histology-controlled study[81] and also in identification of plaques with thin fibrous cap (having high rupture risks)[40]. Additionally, OCT can both assess the effect of coronary artery stenting with BMS, DES and AMS[62, 76] and visualize the complex coronary arterial wall structure after stenting in much greater detail than IVUS[6, 78, 48].

One of the main drawbacks of OCT is its limited penetration depth, which effectively

makes a blood-free environment a requisite for proper imaging. As a non-transparent tissue, red blood cells in the coronary artery cause scattering that results in signal attenuation[7] due to the mismatch of refractive indexes between red blood cells and serum. Several techniques, including balloon occlusion and intra-coronary flush, have been developed to address this limitation and evacuate the blood during examination. While both these techniques have been linked to a risk of ischemia in the examined area, intra-coronary flush has been associated with fewer complications[42]. Alternative methods, including automated catheter pullback at a very high speed and index matching through raising the index of serum, are now under investigation to mitigate these risks[7].

While there are currently no established guidelines for the clinical use of OCT, it has already been applied as the standard of reference in a number of studies: PCI guide and optimization[77], as well as assessment of tissue coverage of stent struts[84], plaque compositon[81] and innovative stent design[61]. Most recently, a study by Yamaguchi et al. demonstrated that OCT is a safe and feasible technique for use in humans, paving the way for its potential to become a gold standard in assessing lumen dimensions of coronary arteries[82].

Histology

Histology is the standard of reference[46, 18, 61] for the validation of in-vivo findings (ie. vessel morphometry and anatomy) in cardiovascular medicine. After the tissue of interest is collected from the subject, it is prepared with a fixative (either chemical or frozen) and stained with an appropriate dye based on the specific question to be answered. The aim of histological staining is to capture microscopic tissue details, and in this study we applied Movat's pentachrome for the comparison of the in-vivo findings[15] because it is a validated method that can reliably assess the vessel both qualitatively and quantitatively[67].

To understand and improve the mechanical stability of AMS, it is imperative to understand their degradation kinetics. In previous studies of degradation kinetics, the immersion and electrochemical tests[32] have been the two most commonly used in-vitro methods, while IVUS and OCT have been the most common in-vivo methods[61]. The immersion test[2] evaluates the corrosion of materials in aqueous solutions by

assessing, for example, their weight over an exposure time. Electrochemical tests on the other hand use an electrolyte solution to measure the oxidation/reduction reactions[1]. Beyond studying the biodegradation of magnesium stents, it is also imperative to capture the distribution of magnesium degradation products within the vessel to quantify their possible adverse effect. However, there is no established method that can answer this question and a histopathological technique that specifically visualizes the magnesium may help us do just that; this was in fact the second specific aim of this study.

Specific Aims

The goal of this study was twofold:

1. To examine the properties as well as possible advantages and disadvantages of intracoronary imaging modalities (i.e. OCT and IVUS) for the assessment of the degradation process of magnesium based biodegradable stents
2. To compare these findings with histology and to develop a histopathologic method to assess the magnesium distribution in the vascular tissue following the degradation process.

Methods

Animals and Procedure

For these studies an animal model with a similar coronary anatomy to that of humans was employed. This model consisted of 4 Gottingen minipigs with a mean age of 24.3 months and a mean weight of 55±3.57 kg. The aim was to implant stents into all three coronary vessels of each pig, using one BMS (bare metal stent) and two AMS (absorbable metal stent) per pig. The assignment of stents to particular vessels was made at random.

To prepare the animals for stent implantation, they were sedated with an intramuscular injection of ketamine (20 mg/kg) and xylazine (2 mg/kg) while intubated and ventilated with oxygen (2 l/min) and isoflurane (1.5 - 3.0%). After a single dose of heparin (150 U/kg) was administered, the femoral artery was cannulated using the Seldinger technique to gain femoral access. Through this access, the stents were deployed using a 6-French (6F) guiding catheter under fluoroscopic guidance into the left anterior descending artery (LAD), the left circumflex artery (LCx), and the right coronary artery (RCA). Points of interest for stenting were vessel segments with a 2.5-3 mm diameter that were also 5 mm away from any branching. Once in position, the stents were expanded to a diameter of 3 mm with the use of a high-pressure balloon at 16 bar (intended balloon to artery diameter ratio of 1.2 – 1.4 was used to induce restenosis by overexpansion of the vessel). Upon completion of stent implantation, a coronary angiography was performed and recorded for precise documentation of stent positioning (along with administration of 0.25 mg of nitroglycerin to prevent possible coronary spasm).

For visualization at the time of stent implantation, IVUS and OCT were performed. Data acquisition was performed during the automated and motorized pullback of the catheter and all images were archived digitally for offline analysis. Potential problems during the examination of the coronary vessel include the automatic pullback, compression, and movement of the fiber optics, which all can reduce the accuracy of dimensional measurements with OCT. To overcome these potential sources of error, both OCT and IVUS probes were calibrated with the aid of a test block.

Once the initial imaging was complete, the femoral access was closed with a dedicated closure device (AngioSeal™, St. Jude Medical, Minnetonka, Minnesota, USA) and the animals were roused from anesthesia. For the next four weeks, they were treated daily with Aspirin (100 mg) and Clopidogrel (75 mg) in order to prevent stent thrombosis.

The next imaging phase was intended at the end of the study, 4 weeks after implantation. The same in-vivo examinations using IVUS and OCT were conducted, along with coronary angiography, on the stented coronary arteries. In order to proceed with ex-vivo imaging the animals were sacrificed and the stents were explanted along with the coronary arteries from the harvested hearts, which were subsequently flushed with an isotonic NaCl solution to clear the remaining blood. The stent-carrying coronary arteries were placed in translucent test tubes and kept in a fluid nitric acid-filled container in order to freeze and preserve them for histology.

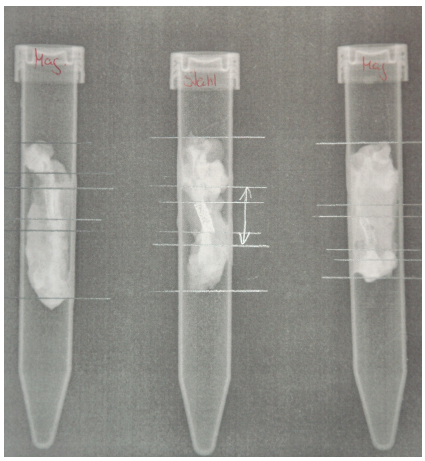

Figure 1: Location of stents with x-ray prior to histology. BMS in the middle; AMS on each side. Before continuing to the planned ex-vivo studies, an x-ray was performed on the thawed stented coronary vessels in order to locate the stents and evaluate their structural integrity. While the low opacity of the AMS made them challenging to visualize, generating an under voltage in the x-ray generator (40 kV and 0.50 mAs) provided adequate images for this evaluation. Figure 1 below displays the resulting x-ray image (BMS in the middle test tube and AMS on each side shown faintly). With x-ray complete, the vessels were refrozen at -80°C.

Coronary Stents

Bare Metal Stents (BMS)

The BMS (PRO-Kinetic, Biotronik, Bülach, Switzerland), used in this study had a diameter of 3mm, length of 10mm and a strut thickness of 60µm (Figure 2). The stents were composed of cobalt chromium with a silicone carbide coating

(PROBIO®), had a double helix design, and were deployed with the use of an expandable balloon catheter.

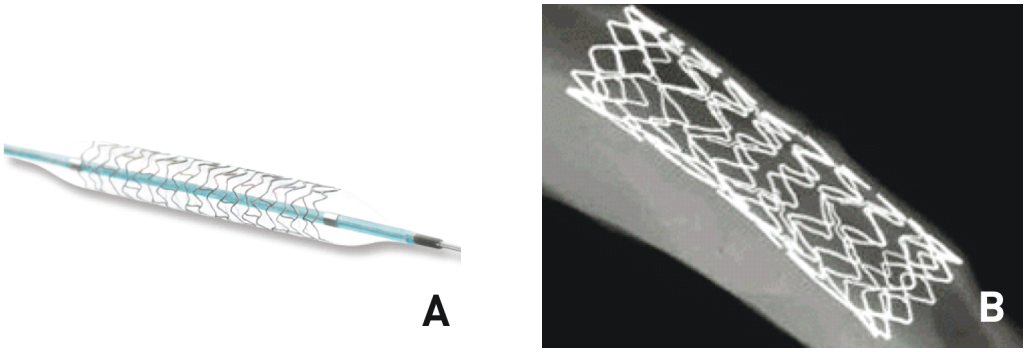

Figure 2: A. PRO-Kinetic cobalt chromium stents before implantation (ex-vivo expanded), B. Low kilo voltage radiographs of porcine coronary arteries implanted with BMS (28 days after implantation)[61].

Magnesium Alloy Stents (AMS)

The AMS (Progress, Biotronik, Bülach, Switzerland) used in this study had wave-shaped segments around their circumference that in turn connected to one another by longitudinal straight segments (Figure 3). The stents are crafted from a single tube using a laser, and are composed of 93% magnesium, 3.7 - 5.5% yttrium, and 1.5 - 4.4% other rare earth elements. Due to its opacity, two radio-opaque markers are attached to the both ends of it. Their complete biodegradation can range from 60 to 90 days[19] depending on the composition of the aforementioned components, and upon degradation resolve to: magnesium-hydroxyappatite, -chloride, -oxide, -sulfate, or -phospate. Animal studies have shown that these products, as well as the stent themselves, are biocompatible[24]. They have a low elastic recoil (<8%) and minimum shortening after inflation (<5%)[19]. Their dimensions were identical to BMS, as was their implantation technique.

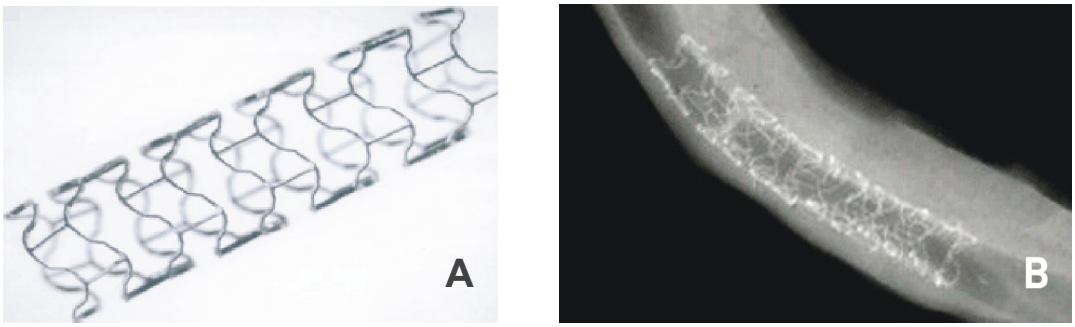

Figure 3: A. AMS before the implantation (ex-vivo expanded), B. Low kilo voltage radiographs of porcine coronary arteries implanted with AMS (28 days after the implantation)[61].

Intravascular Ultrasound (IVUS)

Equipment

The IVUS device, an S5 Imaging System (Volcano Corp., Rancho Cordova, CA, USA, Figure 4A), contains an imaging catheter, a motorized pullback device, an imaging console, and an external signal processing system. The IVUS operates at a frequency of 20-40MHz, provides a resolution of 150-250µm and has a penetration depth of 8mm. The imaging catheter on the device can use one of two different IVUS transducers: a mechanically rotating transducer, or an electronically switched multi-element array system. The one used in this experiment, an Eagle Eye Gold Catheter (Volcano Corp., Rancho Cordova, CA, USA, Figure 4B) uses the latter. The catheter employs an angiography guide wire that allows for intracoronary insertion, and uses a 64-element transducer with an array of crystal situated annularly at the edge of the imaging catheter itself. One set of the elements in this array transmits the sound, while a second set receives it simultaneously[49].

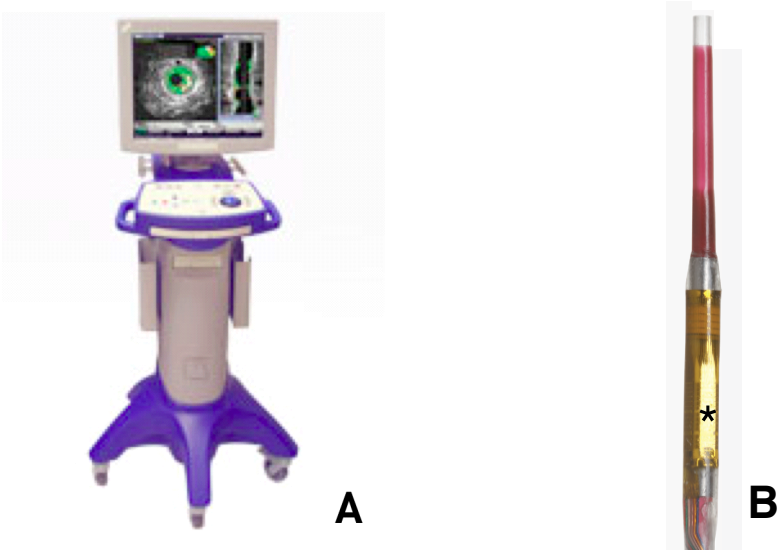

Figure 4: A. IVUS S5 Imaging System (Volcano Corp., Rancho Cordova, CA, USA), B. Eagle Eye Gold Catheter (Volcano Corp., Rancho Cordova, CA, USA) with multi element array system transducer (∗).

Study

For visualization at time of stent implantation, an IVUS catheter was placed with the use of a guiding catheter at the distal end of the stent in the implanted coronary artery under fluoroscopic guidance. In order to scan the vessel lengthwise, the catheter-imaging tip was pulled back at an automatic constant speed between 0.5 mm/s (Trak

Back II, Volcano Corp., Rancho Cordova, CA, USA). Thanks to the electronic transducer system used no non-uniform rotational distortion (NURD) artifacts could occur. Ring-down artifacts – bright halos of variable thickness surrounding the catheter – can be removed automatically by using the integrated NearVu software. The acquired data was archived in the DICOM (digital imaging and communications in medicine) format for offline studies.

To compare IVUS, OCT, and histology, images from each millimeter of the stented areas were used (eleven cross-sectional images).

Dimensions

- Stent area (mm^2): Area between connecting lines of the outer and inner edges of the stent.
- Min lumen diameter (mm): Minimum diameter of the lumen-intima border
- Max lumen diameter (mm): Maximum diameter of the lumen-intima border
- Strut number (#): Number of stent struts within a cross-section
- Strut thickness (mm): Mean axial diameter of 3 randomly chosen struts from each cross-section

Analysis Software

Images acquired with IVUS were analyzed using Tape Measure (Indec Systems, Mountain View, CA, USA), a commercially available software for the computerized planimetry of coronary arteries. The images acquired with IVUS were imported into Tape Measure and were calibrated using a raster from the image data. The exact location of each image was determined by using the time display on the image and known pullback rate of the catheter.

Optical Coherence Tomography (OCT)

Equipment

Similar to IVUS, the equipment for the intracoronary OCT System (M2 LightLab Imaging Inc., Westford, USA, Figure 5) consists of an imaging catheter, a motorized pullback device, an imaging console (containing light source), signal processing units, data storage and display. The OCT uses broadband infrared light with a wavelength of 1300±50 nm. Its resolution is 15 μm and it has a penetration depth of 2mm.

Figure 5: OCT System (M2 LightLab Imaging Inc., Westford USA)

An over-the-wire occlusion catheter (Helios, Goodman &Co. LTD., Japan, Figure 6) was used to clear the examined coronary artery of blood. The inside of the occlusion catheter was hollow, allowing not only for the insertion of the guiding catheter and the OCT imaging catheter, but also for the segment of interest to be flushed with the isotonic NaCl or Ringer's Lactate solution. During imaging, the low-pressure occlusion balloon catheter is positioned proximal to the examined segment and is inflated at 0.3atm. Simultaneously, the coronary blood flow is evacuated by continuous flush of isotonic NaCl solution. The vessel occlusion time is limited to 30 seconds to avoid any ischemia or arrythmia.

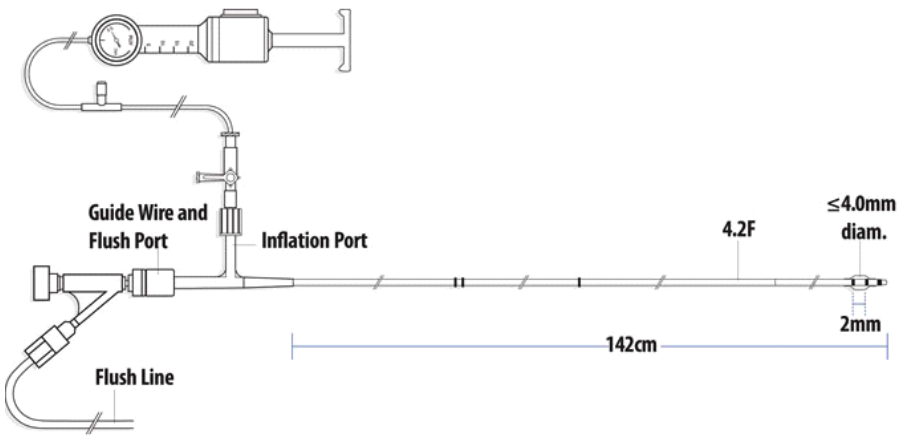

Figure 6: Schematic illustration of occlusion balloon catheter (Helios, Goodman & Co. LTD. Japan).

The imaging catheter (Imaging Wire, LightLab Imaging Inc. Westford, USA) contains a translucent casing that itself contains a single-mode optical fiber. The tip of the catheter directs the optical signal with the use of a microprism lens at the vessel wall. Additionally, the catheter has a 15mm radiopaque tip situated slightly away from its distal segment in order to identify its position as it lacks adequate opacity under fluoroscopy. As the imaging catheter rotates and is retracted (at 1 mm/s) from the coronary artery, a tomographic cross-sectional image is captured along a length of 30nm in a single run.

Study

Upon completion of IVUS, the over-the-wire occlusion balloon catheter of the OCT was placed over the same guiding catheter and slid to the stented segment. The guiding catheter was then removed, and the imaging probe of the OCT was inserted through the lumen of the occlusion balloon distal to the segment of interest. To prepare for clearing the coronary vessel of blood, the occlusion balloon was then pulled back into the proximal segment. Just prior to image acquisition, the balloon was inflated to 0.3 bar to block blood flow, and a solution of isotonic NaCl at body temperature was flushed through the end-hole of the occlusion balloon catheter to evacuate the blood remaining in the coronary artery. Once cleared of blood, the imaging probe visualized the stented vessel as it was removed distally at a speed of 1 mm/s. All acquired OCT images were archived digitally for offline examination.

Dimensions & Analysis

The same dimensions as IVUS were also acquired for OCT images. This data was analyzed similarly to IVUS with Tape Measure (Indec Systems, Mountain View, CA, USA).

Histology

Movat's Pentachrome Stain (MPS)

Equipment

The pentachrome stain was originally developed by Movat in 1955 as a single histochemical stain to isolate and visualize the different components of tissue[51]. The major elements of MPS are: Verhoeff elastic hematoxylin, sodium thiosulfate, acetic

acid, alcian blue, crocein, scarlet–acid fuchsin and alcoholic saffron solutions[66]. MPS enhances vessel wall structure, especially the elastin and smooth muscle components[67], and in doing so facilitates detection of otherwise easy-to-miss vascular pathology.

Study

The stented coronary vessels were prepared for the histological study with the aid of cryosectioning, a technique used to cut tissue in frozen state with a microtome knife within a cryostat. The advantage of the cryosectioning procedure over using a fixative is that the frozen tissue degrades much slower and does not alter nor mask its chemical composition as much. The vessel of interest was placed on a metal tissue disc that is then secured in a chuck. The specimen is then embedded in a gel like medium consisting of poly ethylene glycol and polyvinyl alcohol; this compound has the same density as frozen tissue when frozen. With the use of a standard steel microtome knife, the frozen coronary vessels with implanted AMS were sliced into 10μm-thick segments, starting 5mm proximal of the stented segment to 5mm distal to it (resulting in 200 segments, as the stents were 1 cm). The segments were mounted on glass slides, photographed (AxioCam HRC, Carl Zeiss Germany) in a native state, then stained (see Figure 7) with Movat's pentachrome as described in the following paragraph and then re-photographed to isolate any morphology changes attributable to the staining procedure. All images were archived in jpeg format.

The slides were first left to dry in ambient air overnight. Then, after fixation in a 70% alcohol bath for five minutes, they were left to air-dry for another 30 minutes and finally photographed in their native state.

The staining procedure employed was a small modification to Movat's Pentachrome stain that minimized the corruption of AMS due to water and alcohol:

The staining began with hydration to distilled water for three minutes to remove any remaining alcohol[45]. After pre-treating the slides in acetic acid (3%) for 30 seconds, they were placed for 30 minutes in alcian blue (Sigma) to stain the ground substance. Upon washing off the rest of this stain under running water for 1 minute, the staining continued in the Vorheoff's solution for nine minutes, in order to differentiate the elastic fibers and nuclei. The Vorheoff's Stock solution consisted of four different

solutions that have to be made fresh daily. The working solution uses orcein (Merck) and hematoxylin (Sigma) as dyes. The slides were then dipped in in 1% aqueous ferric chloride (Merck) for one minute to differentiate. Upon being rinsed briefly in running water, the slides were then placed in the crocein scarlet-acid fuchsin (Fluka) (consisting of 2 separate solutions: crocein scarlet and acid fuchsin) for three minutes to stain the muscles and fibrin, and then rinsed in acetic acid (1%) to fixate. Then the slides were differentiated in 2% aqueous phosphotungstic acid for 15 min. The phosphotungstic acid was removed with the use of 1% acetic acid. After dehydrating in 100% alcohol for two minutes, the slides were stained in saffron for 6 minutes to stain the reticular fiber and collagen to yellow, followed finally by dehydration in 100% alcohol for five minutes and mounted in entellan (Merck) and Canada balsam.

As it has been shown in many studies that the different phases of histological preparation often affects the dimensions of coronary arteries[17,10], in order to determine the effect of staining on the vessel morphometry for this study both native and stained cross-sectional images were compared.

For intra-observer reproducibility, one observer repeated an identical analysis on the histological segments after an interval of three months.

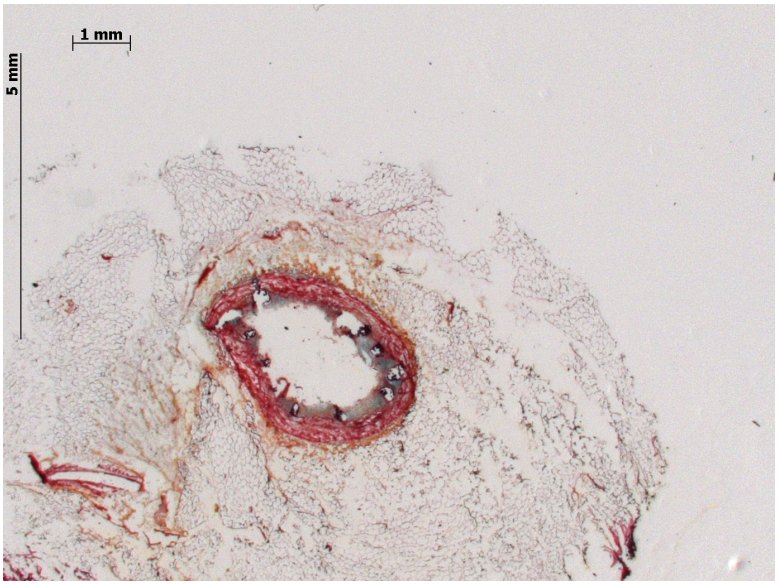

Figure 7: Scaled for histological vessel morphometry (AxioCam HRC, Carl Zeiss Germany). Colors are as follows: Nuclei and elastic fibers are black, collagen and reticular fibers are yellow, ground substance and mucin are blue, fibrinoid and fibrin are intense red, and the muscle is red.

Dimensions

- Min lumen diameter (mm): Minimum diameter of the lumen-intima border
- Max lumen diameter (mm): Maximum diameter of the lumen-intima border
- Mean lumen diameter (mm): Mean diameter of the lumen-intima border
- Strut number (#): Number of the stent struts in a cross section
- Strut area (mm^2): Area of a stent strut
- Lumen area (mm^2): inner area left between lumen-intima border
- Intima area (mm^2): area between intima-media border
- Vessel area (mm^2): area between media-adventitia border

Analysis Software

AxioVision (Carl Zeiss Inc., Germany) was the software used to perform the planimetry of the histology samples. Images of the samples were acquired directly from the microscope thanks to its integrated camera controls. The software's interactive histogram and image processing tools helped to optimize color and contrast. Because the software reads and writes in ZVI-format, the digital images are processed and saved with a loss-free wavelet algorithm, meaning the images are uncompressed in contrast to generic file formats like TIF or JPEG. The ZVI format also ensures that other pertinent information, e.g. annotations or magnification, is also saved along with the pixel data in a single file (Carl Zeiss).

Titan Yellow Stain

Equipment

Titan yellow is a triazene dye used as a stain and fluorescent indicator that helps to detect magnesium[70]. The stain changes its color from yellow to orange/red in the presence of magnesium.

In 1927, Kolthoff described magnesium's reddish-orange appearance upon reaction with alkaline solutions[44]. Later in 1951, Craig used the same method to detect magnesium in serum and plasma[13]. Glick, Freier and Ochs were later able to detect magnesium in adrenal glands with the use of a photometric micro-procedure[27]. More recently, in 1991, Müller and Firsching demonstrated that Titan yellow reliably detects magnesium in tissues with elastic fibers[51].

In this study we applied this method to detect and demonstrate the biodegradation of

the magnesium alloy stents. The major components of this stain were titan yellow solution (5% thiazole yellow, and sodium hydroxide NaOH), Weigert's resorcin and orcein. While Weigert's resorcin and orcein are not standard components of the Titan yellow stain, we employed them in this study in order to provide a strong contrast to better isolate the orange/red color of the magnesium.

Procedure

Once the slides were prepared with the use of cryosectioning they were photographed in their native state, hydrated with distilled water for 15 minutes, fixed in a 70% alcohol bath for five minutes, and then placed in the Titan yellow solution for 20 minutes. After rinsing the slides with distilled water they were immersed in the Weigert's resorcin solution for three minutes, and then washed under running water. Finally, the slides were immersed in the orcein solution for two minutes to complete the staining. The slides were differentiated first as follows: in 96% alcohol, 100% alcohol and xylol each for five minutes and then mounted with Vectashield®. As mentioned before, magnesium is indicated by an orange-red color and this reaction occurs within minutes. The stained slides were visualized with the aid of a fluorescence microscope (Zeiss Axiotech Vario, Germany), photographed with a camera (AxioCam HSm, Carl Zeiss Germany), and filtered for DAPI (excitation at 360 nm and emission at all wavelengths) to examine the biodegradation process (Figure 8). We were not interested in vessel morphometry.

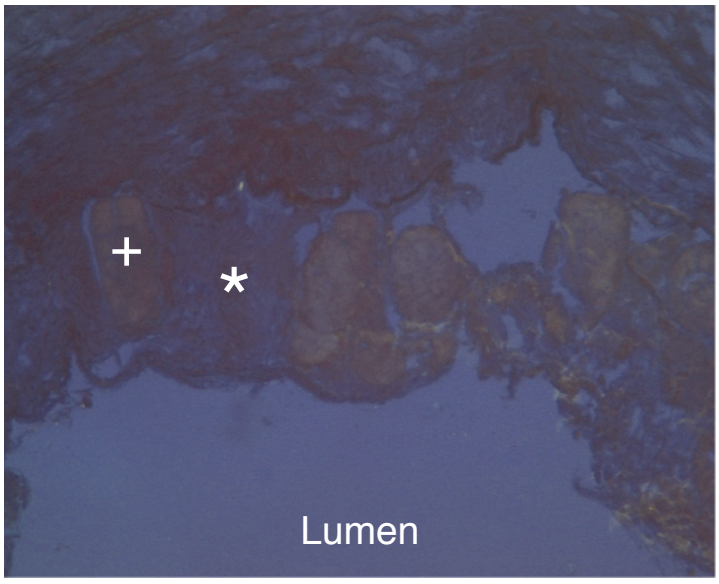

Figure 8: Titan yellow stained struts on a cross-section. Notice the orange-yellow colored AMS struts (+) surrounded by a thin endothelial coverage (*). Photographed on fluorescence microscope (Zeiss Axiotech Vario, Germany) with camera (AxioCam HSm, Carl Zeiss Germany) and DAPI filter.

Statistics

Statistical analysis was performed using SPSS 12.0.1 for Windows (SPSS, Chicago, IL, USA). The ANOVA-Test was used to compare dimensions between BMS and AMS, while the Bland-Altman approach was used to make comparisons between different imaging techniques. The significance level was determined to be 1% and 5% respectively.

Results

Animals and Study

For this study, four Gottingen minipigs were implanted with ten stents: 3 Bare Metal Stents (BMS) and 7 Magnesium Alloy Stents (AMS). Table 1 gives an overview of the assignment of these stents. Two animals received three stents each, while two others received just two due to complications. Upon implantation of its second stent, Animal 92872 developed a ventricular tachycardia that was successfully treated, resulting in the third stent not being implanted as planned. Animal 73535 died during OCT imaging after implantation of two stents into its LAD and LCx. In order not to compromise the study, we did not continue with OCT imaging of the remaining two animals. At the time of the implantation, eight stents were assessed with the use of IVUS and two with OCT.

After four weeks, IVUS and OCT visualization was repeated on the three remaining animals. Only seven out of the eight vessels could be studied with both IVUS and OCT, resulting in four AMS and three BMS being imaged. One stent in the LAD of animal 92872 could not be visualized prior to explantation due to the vessel being dissected and occluded during OCT at implantation.

Upon completion of in-vivo imaging, the animals were sacrificed and their hearts were harvested for histological study.

Animal	Vessel	Stent
92872	RCA	-
	LAD	AMS
	LCx	BMS
73448	RCA	AMS
	LAD	AMS
	LCx	BMS
92879	RCA	AMS
	LAD	AMS
	LCx	BMS
73535	RCA	-
	LAD	AMS
	LCx	AMS

Table 1: Animal assignment of BMS & AMS implantation by vessel.

Implantation

IVUS

At implantation, eight stents were studied with the use of the IVUS: 3 BMS and 5 AMS. The stent struts of both AMS and BMS were presented similarly, both echogenic with a distal acoustic shadowing. However, the echogenicity was lower for AMS. Neither stent type displayed any malapposition, dissection, thrombus or neointima formation (Figure 9).

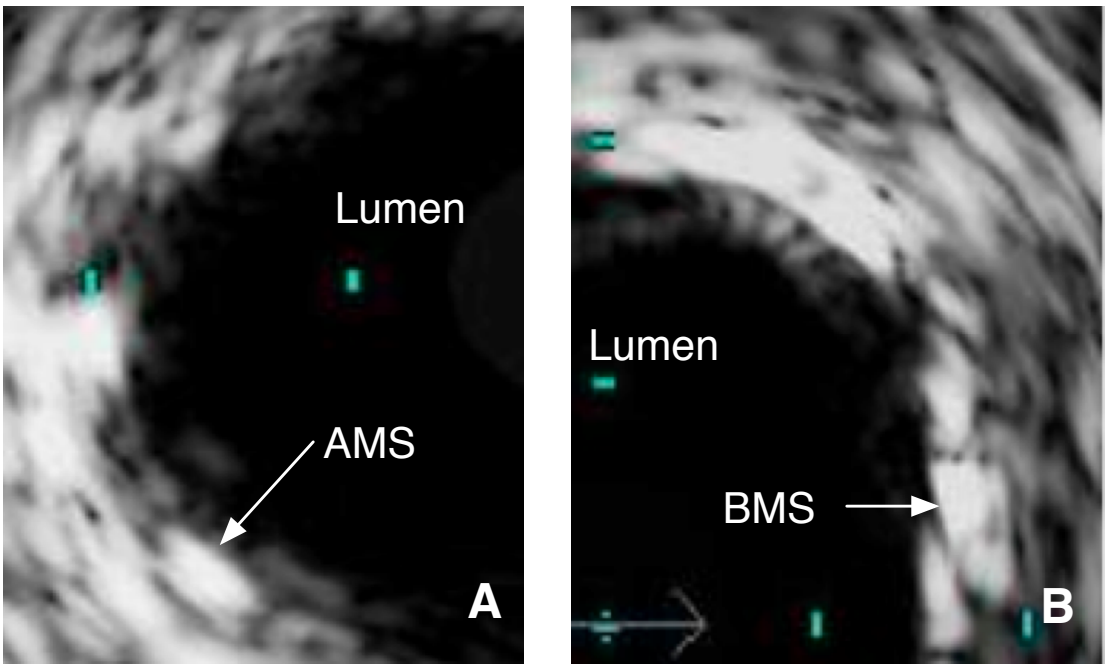

Figure 9: IVUS images of AMS (A) and BMS (B) at the time of implantation. The stent struts of both AMS and BMS were presented similarly, both echogenic with a distal acoustic shadowing. Neither stent type displayed any malapposition, dissection, thrombus or neointima formation.

The following parameters were assessed with IVUS on the five AMS and three BMS: stent area, strut number, strut thickness and min and max lumen diameter. The mean value of each parameter can be found in Table 2.

OCT

As explained earlier, only two vessels could be imaged with OCT during implantation: one AMS and one BMS. Both stent struts presented as bright and highly reflective bands with distal shadowing. The AMS struts appeared slightly thicker than BMS struts, and had a better signal intensity. Contrary to the IVUS results, the cross-sectional OCT images displayed an incomplete apposition in both AMS and BMS

(Figure 10). Due to the limited number of samples, no standard deviation was calculated for this series.

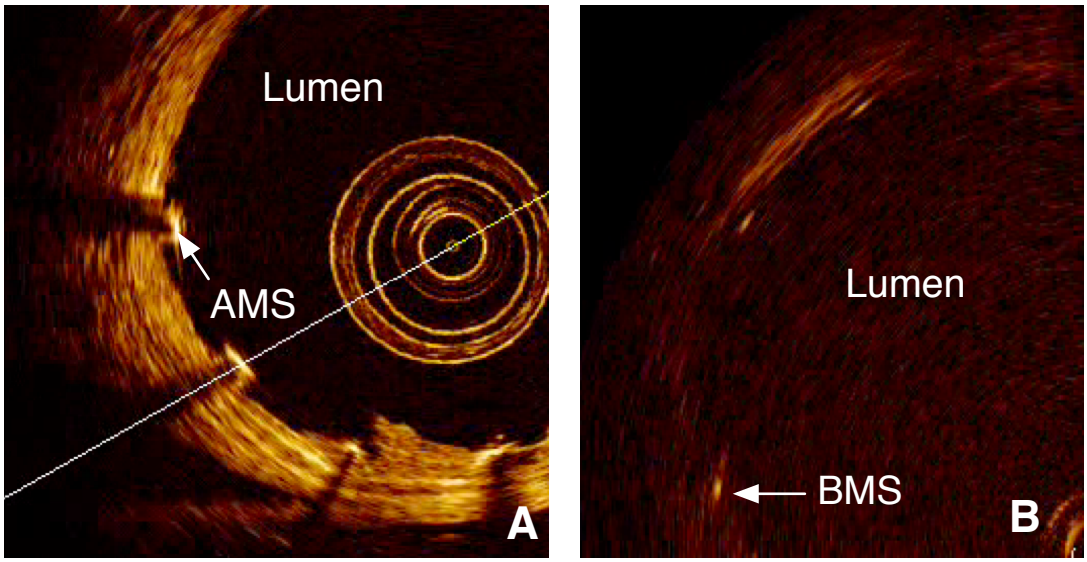

Figure 10: OCT images of AMS (A) and BMS (B) at the time of implantation. The AMS struts appeared slightly thicker than BMS struts, while both clearly displayed distal acoustic shadowing. Contrary to the IVUS results, the cross-sectional OCT images displayed an incomplete apposition in both AMS and BMS.

Similar parameters to IVUS were assessed with OCT: stent area, strut number, strut thickness, and min and max lumen diameter. Unlike in IVUS, no standard deviation was calculated due to the limited numbers of stents assessed. The mean values of the parameters are shown in Table 2.

Technique	Type	Parameter	Visualized Stents	Mean Value	Standard Deviation
IVUS	AMS	Stent Area	5	8.00	1.05
		Strut Number	5	6.38	1.22
		Strut Thickness	5	0.20	0.03
		Max Lumen Diameter	5	3.16	1.19
		Min Lumen Diameter	5	2.88	0.19
	BMS	Stent Area	3	6.31	0.66
		Strut Number	3	8.88	2.18
		Strut Thickness	3	0.19	0.03
		Max Lumen Diameter	3	2.84	0.16
		Min Lumen Diameter	3	2.59	0.14
OCT	AMS	Stent Area	1	8.40	n.a.
		Strut Number	1	8.00	n.a.
		Strut Thickness	1	0.05	n.a.
		Max Lumen Diameter	1	3.35	n.a.
		Min Lumen Diameter	1	3.09	n.a.
	BMS	Stent Area	1	8.1	n.a.
		Strut Number	1	4.55	n.a.
		Strut Thickness	1	0.04	n.a.
		Max Lumen Diameter	1	3.31	n.a.
		Min Lumen Diameter	1	3.03	n.a.

Table 2: Overview of morphometric parameters with IVUS und OCT during implantation

Explantation

IVUS

At the time of explantation, there was no visible change in the appearance of BMS with IVUS. The AMS struts on the other hand showed clear signs of degradation, with a fainter appearance and a decline in distal acoustic shadowing. Some AMS struts could barely be discerned from the vessel wall, and complete endothelial

coverage of struts was not visible (Figure 11).

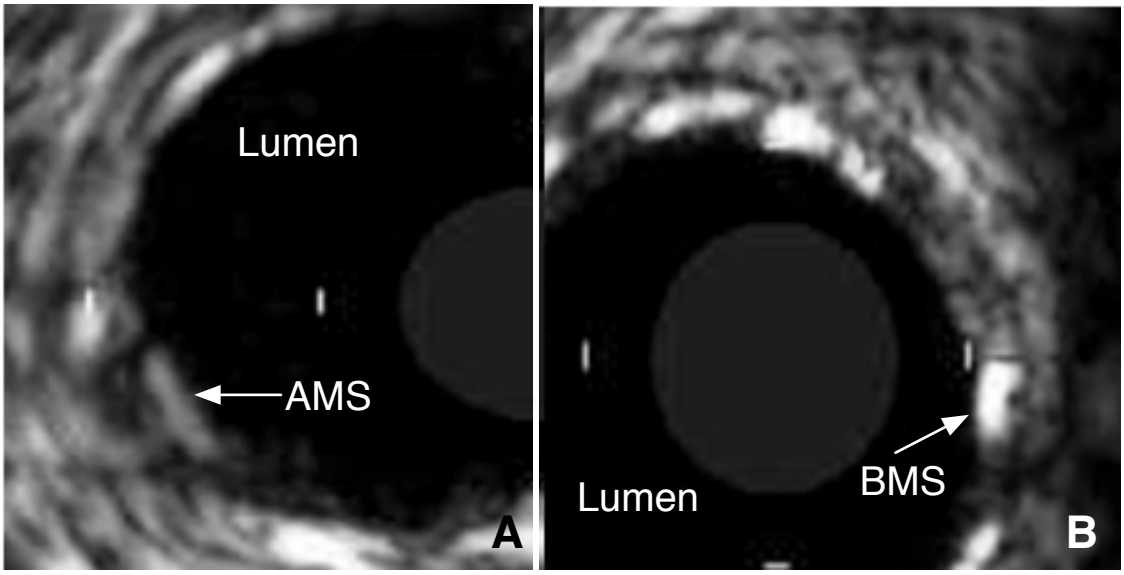

Figure 11: IVUS images of AMS (A) and BMS (B) at the time of explantation. There was no visible change in the appearance of BMS with IVUS. The AMS struts on the other hand showed clear signs of degradation, with a fainter appearance and a decline in distal acoustic shadowing. Some AMS struts could barely be discerned from the vessel wall, and complete endothelial coverage of struts was not visible.

The same parameters assessed at time of implantation were also assessed at the time of explantation (stent area, strut number, strut thickness, and min and max lumen diameter) for both AMS (four stents) and BMS (three stents). The mean value of each parameter in the IVUS is shown in Table 3. While no change was observed in BMS, the AMS stent area was significantly reduced (26%) over those 4 weeks. The strut number and strut thickness were also both reduced (30% and 30% respectively), and both the min and max lumen diameters were also reduced minimally (16% and 3%) (Table 4).

OCT

Seven vessels, the same amount as with IVUS, were analyzed with OCT: four AMS and three BMS. At the time of explantation, the incomplete apposition present at implantation was no longer apparent and there was thin endothelial coverage of the stent struts. Again the BMS appeared unaltered compared to implantation, while the appearance of the AMS was noticeably changed. AMS struts appeared darker and more diffuse. Some struts seemed to have dissolved and had less discernible distal shadowing (Figure 12). Due to the limited numbers of studies during implantation, a comparison between OCT at implantation and explantation was not feasible.

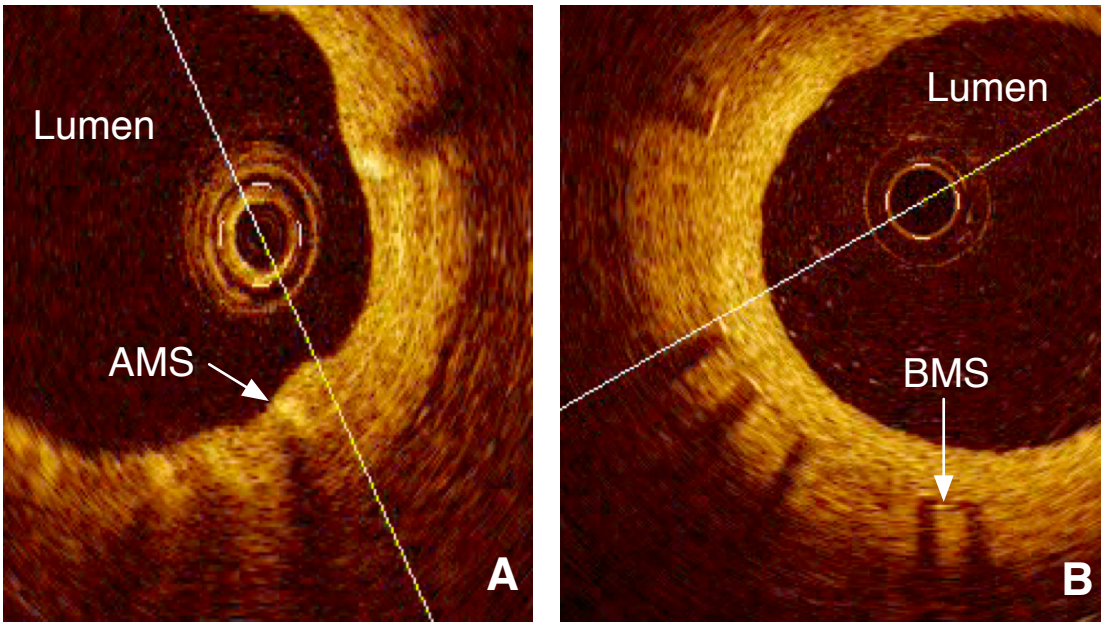

Figure 12: OCT images of AMS (A) and BMS (B) at the time of explantation. The incomplete apposition present at implantation was no longer apparent and there was a thin endothelial coverage of the stent struts. Again the BMS appeared unaltered compared to implantation, while the appearance of the AMS was noticeably changed. AMS struts appeared darker and more diffuse. Some struts seemed to have dissolved and had less discernible distal acoustic shadowing

The same parameters were assessed at the time of implantation as at the time of explantation with OCT. Due to the limited number of vessels at the time of implantation, no comparison was made between the dimensions at the time of implantation and explantation. The mean value of each parameter in the IVUS is shown in Table 3.

Histology

Movat's Pentachrome Stain (MPS)

This ex-vivo study allows one to visualize AMS stented vessels. Three layers of vessel wall could be identified with the use of this stain. As indicated in methods, the endothelium surrounding the struts was displayed in blue, the vessel layers in red with varying intensity (based on composition of muscle and fiber), the adventitia in yellow (collagen), internal and external lamina elastic, and struts, were captured in black (Figure 13). The high resolution of MPS enables vessels to be assessed in detail and helps capture thrombus (Figure 14A, B) and neointima formation (Figure 15A, B, C) that could otherwise not be detected using another of the imaging techniques.

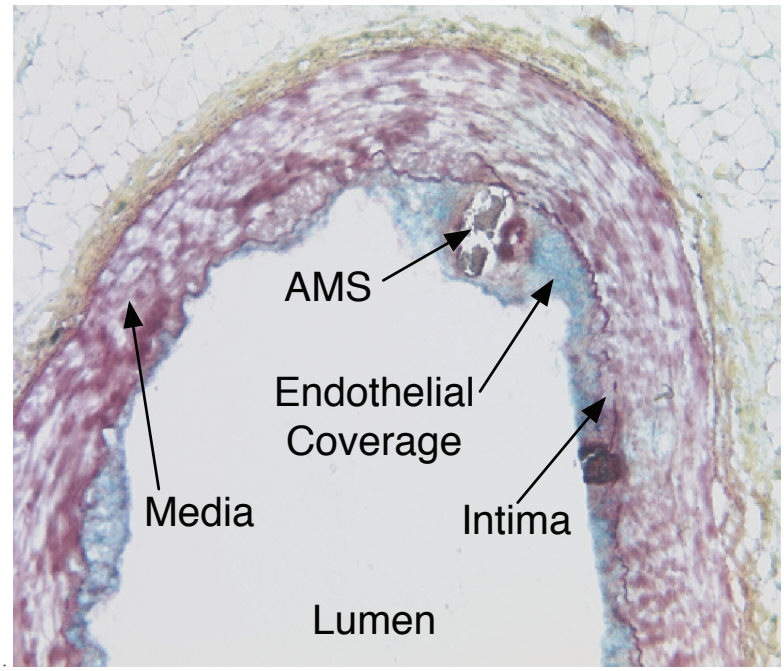

Figure 13: Three layers of vessel wall could be identified with the use of the stain. As indicated in the methods: the endothel surrounding struts was displayed in blue, the vessel layers in red with different accentuation (based on its content of muscle and fiber), the collagen around adventitia in yellow (collagen), the internal lamina elastica, external lamina elastica and struts in black (AxioCam HRC, Carl Zeiss Germany).

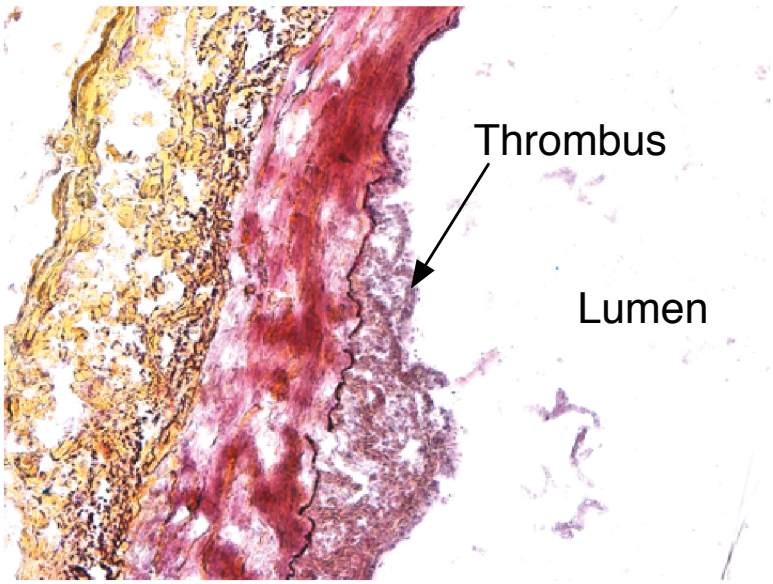

Figure 14A: A platelet-rich thrombus adherent to the lumen. Histology was the sole method employed in this study to visualize thrombus formation (AxioCam HRC, Carl Zeiss Germany).

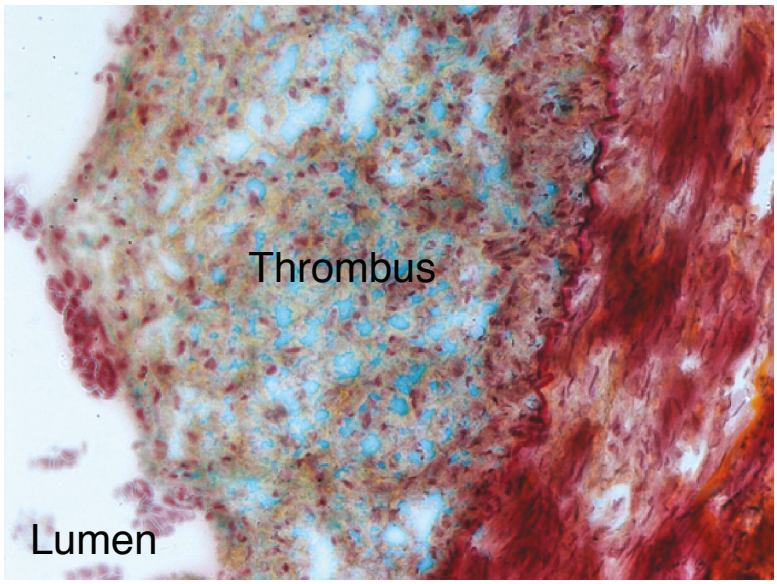

Figure 14B: Note the platelets on the top of a complex of smooth muscle cells in a collagenous matrix. Due to its high resolution and this specific staining technique, vessel pathology could be reliably visualized (AxioCam HRC, Carl Zeiss Germany).

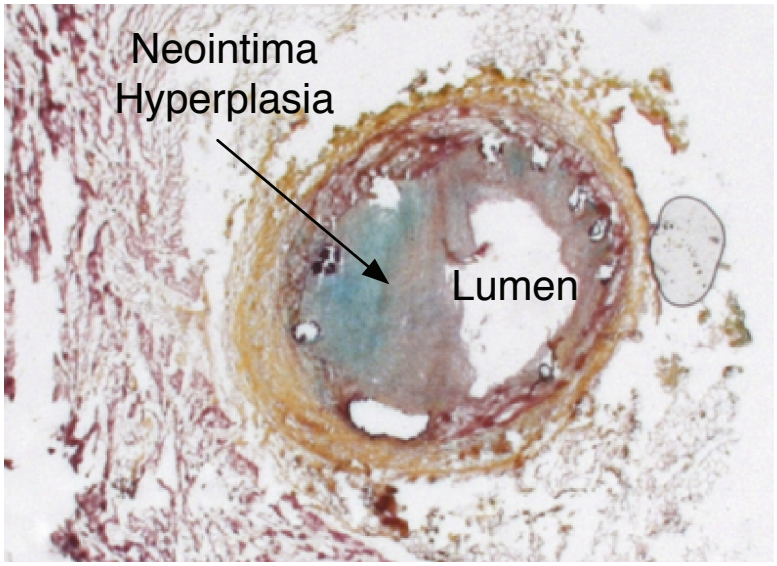

Figure 15A: Eccentric lumen obstruction due to neointima hyperplasia (ie. migration of smooth muscle cells, platelets, leucocytes, and proliferation of extra cellular matrix) as a result of arterial wall injury after stent implantation (AxioCam HRC, Carl Zeiss Germany).

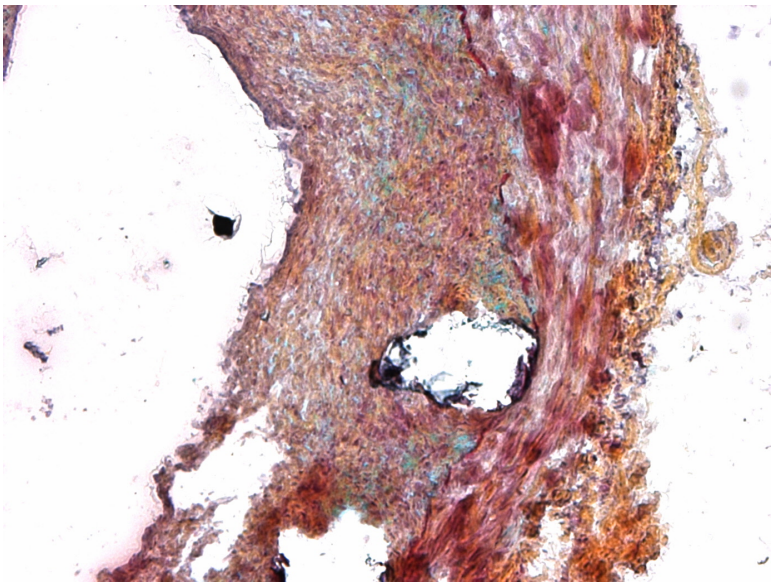

Figure 15B: A magnified section from Figure 15A. Note the smooth muscle cells (red) surrounding the struts.

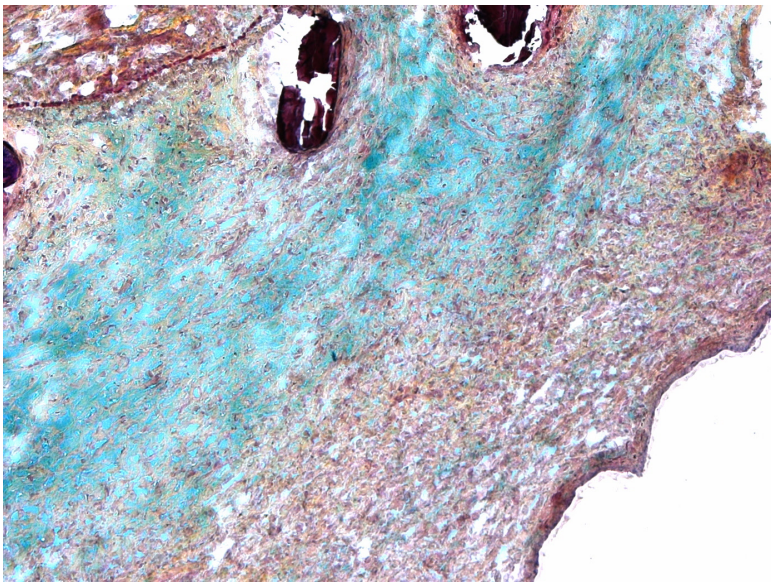

Figure 15C: Another magnified section of Figure 15A. Note the collagenous matrix (blue) produced by smooth muscle cells (AxioCam HRC, Carl Zeiss Germany)

Due to technical difficulties, only AMS could be studied at the time of explantation. As a result of the histological processing, some struts were washed out so that there was no constancy among strut numbers at different positions. Additionally, a few samples were destroyed during the preparation, further reducing the number of cross-sections from 33 to 19 available to study (Figure 16).

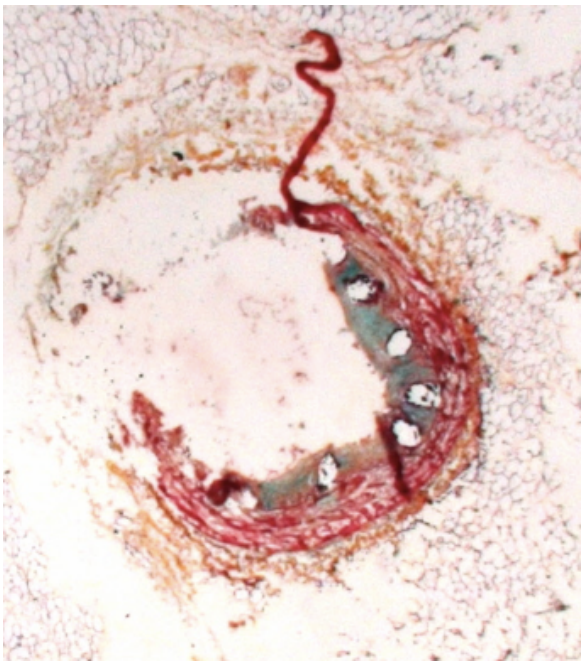

Figure 16: As result of the histological processing, a few samples were destroyed during preparation, further reducing the number of cross-sections available. Note also the wash-off effect of staining on the struts as seen by the empty strut lobes (AxioCam HRC, Carl Zeiss Germany)

The maximum lumen diameter ranged from 1.10-2.32 mm with a mean value of 1.75±0.29 mm. The minimum lumen diameter varied between 0.038-1.42 mm for a mean of 0.85±0.31 mm. For strut number, the mean value was determined to be 7.5±2.17 while ranging from 3 to 25. And the mean strut area for was 0.03±0.01 mm^2 while varying between 0.02-0.06 mm^2 (Table 3).

Technique	Stent Type	Parameter	Stents	Mean Value	Standard Deviation
IVUS	AMS	Stent Area	4	5.93	0.48
		Strut Number	4	4.45	1.47
		Strut Thickness	4	0.15	0.02
		Max Lumen Diameter	4	2.88	0.46
		Min Lumen Diameter	4	2.69	0.37
	BMS	Stent Area	3	6.36	0.57
		Strut Number	3	9.42	1.87
		Strut Thickness	3	0.19	0.24
		Max Lumen Diameter	3	2.69	0.31
		Min Lumen Diameter	3	2.55	0.43
OCT	AMS	Stent Area	4	4.33	1.59
		Strut Number	4	6.20	2.08
		Strut Thickness	4	0.05	0.006
		Max Lumen Diameter	4	2.53	0.60
		Min Lumen Diameter	4	2.16	0.63
	BMS	Stent Area	3	7.81	0.39
		Strut Number	3	5.85	2.43
		Strut Thickness	3	0.04	0.006
		Max Lumen Diameter	3	2.45	0.53
		Min Lumen Diameter	3	2.14	0.44
Histology	AMS	Max Lumen Diameter	3	1.75	0.29
		Min Lumen Diameter	3	0.85	0.31
		Strut Number	3	7.5	2.17
		Strut Area	3	0.03	0.01

Table 3: Overview of the dimensions in IVUS, OCT, CT and histology at the time of the explantation.

Stent	Parameter	Implantation			Explantation			% Change
		Stents	Mean Value	SD	Stents	Mean Value	SD	
AMS	Stent Area	5	8.00	1.05	4	5.93	0.48	- 26
	Strut Number	5	6.38	1.22	4	4.45	1.47	- 30
	Strut Thickness	5	0.20	0.03	4	0.15	0.02	- 30
	Max Lumen Diameter	5	3.16	1.19	4	2.88	0.46	- 16
	Min Lumen Diameter	5	2.88	0.19	4	2.69	0.37	- 3

Table 4: IVUS measurement comparison for AMS at implantation vs. explantation.

Titan Yellow Stain

Titan yellow stain was used to evaluate the bioabsorble struts separately (not the vessel layers) and also to observe/understand the biodegradation process. The titan yellow study was performed on 90 randomly chosen cross-sections of vessels stented with AMS. To avoid washing out the biodegradable stent struts, the staining procedure was modified so that the time for dehydration in ethanol baths was minimized. Under fluorescence microscopy the struts appeared orange, while the embedded endothelium appeared bluish-violet due to the combined staining with Weigert's resorcin and orcein (Figure 17A, B).

This method demonstrated the diffusion of the AMS degradation products to the surrounding tissue. Due to technical difficulties with the fluorescence microscope, only 25 cross-sections out of the original 90 could be studied. And 12 out of those 25 cross-sections captured the diffusion of degradation products in to the surrounding tissue.

Upon taking this study up again 3 months later, the stain was no longer strong enough to capture diffusion of the magnesium particles – only strong enough to identify the struts. Due to the variation of staining quality, no quantitative analysis of diffusion was possible (Figure 18).

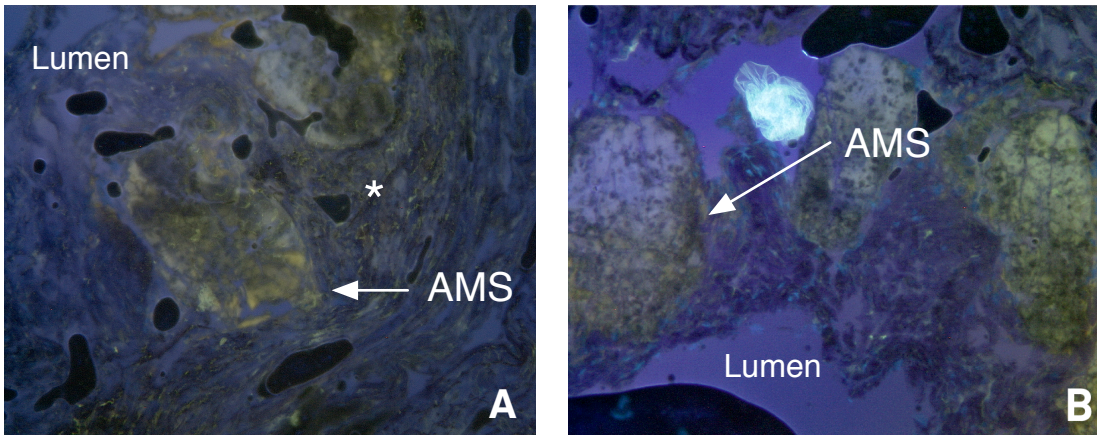

Figure 17A,B: Note the yellow magnesium struts surrounded by bluish-violet displayed endothelium. The yellow hue (*) around the AMS struts demonstrates the diffusion of the magnesium into the surrounding tissue. Photographed on a fluorescence microscope (Zeiss Axiotech Vario, Germany) with a camera (AxioCam HSm, Carl Zeiss Germany) and DAPI-filter.

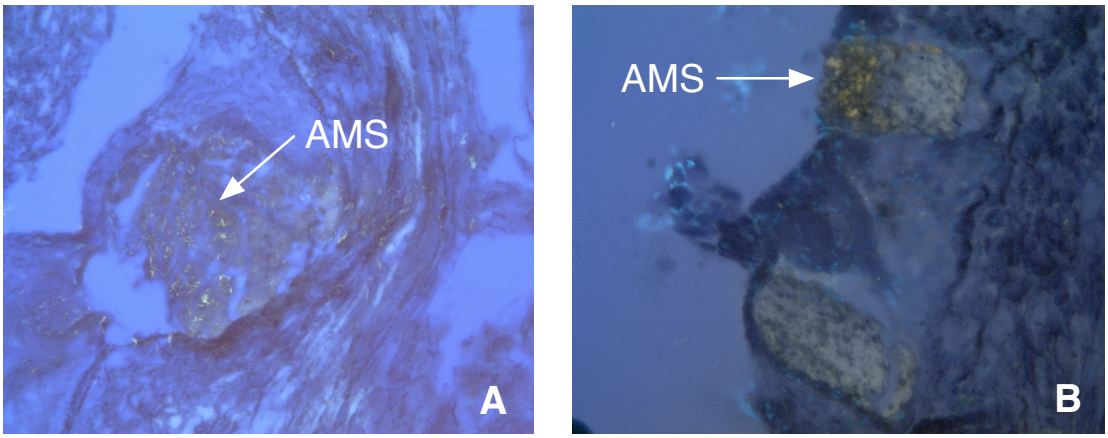

Figure 18A,B: The stain was no longer strong enough to capture the diffusion of the magnesium particles, but strong enough to identify the struts. Photographed on a fluorescence microscope (Zeiss Axiotech Vario, Germany) with a camera (AxioCam HSm, Carl Zeiss Germany) and DAPI-filter.

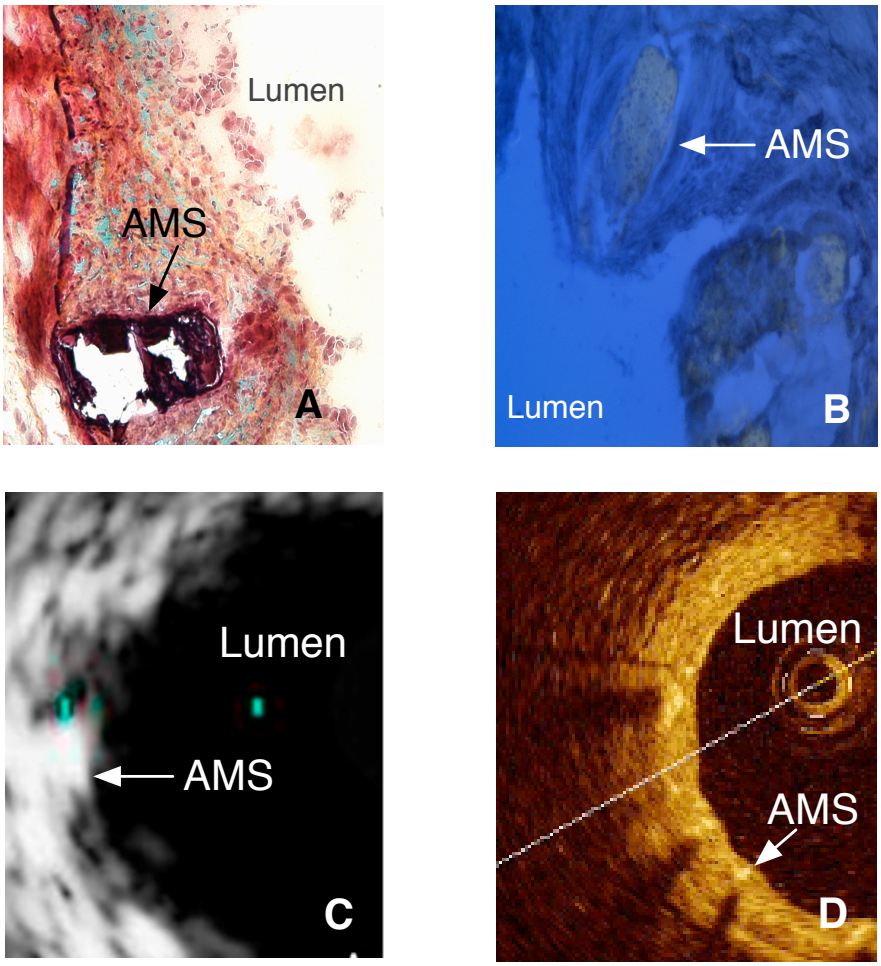

Figure 19: Overview of the four different visualization techniques at time of explantation. (A) MPS: Single black AMS strut partially dissolved due to processing, is embedded within a thin endothelial coverage. (B) Titan yellow: Selective demonstration of AMS – note the yellow AMS on a bluish-violet background. (C) IVUS: Clear signs of degradation of the AMS, with a fainter appearance and a decline in distal acoustic shadowing. (D) OCT: AMS struts appear darker and more diffuse than at implantation – some struts seemed to have dissolved and had less discernible distal acoustic shadowing.

Comparison of Imaging Techniques

In-vivo: IVUS vs. OCT

Both IVUS and OCT showed a qualitative indication of biodegradation by means of a signal reduction of AMS (Figure 20). With IVUS, the AMS appeared fainter and had less distal acoustic shadowing. Some AMS struts could barely be discerned from the vessel wall. With OCT, the AMS struts appeared darker and more diffuse. Some struts seemed to have dissolved, and had less discernible distal shadowing. OCT was also able to capture the endothelial coverage, stent apposition and neointima formation.

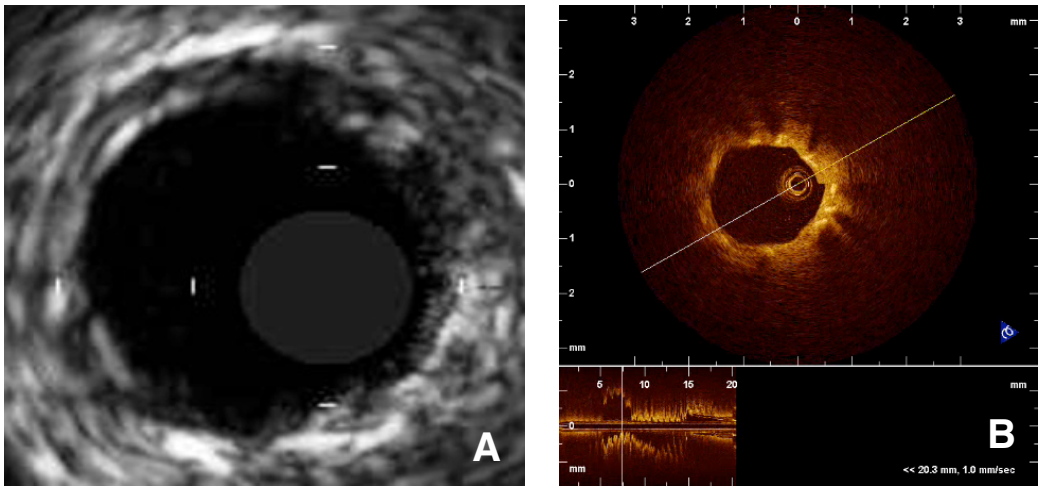

Figure 20: With IVUS (A), the AMS appeared fainter with less distal acoustic shadowing. With OCT (B), the AMS struts appeared darker and more diffuse. Some struts seemed to have dissolved, and had less discernible distal acoustic shadowing. OCT was also able to capture the endothelial coverage, stent apposition and neointima formation.

Due to the limited analysis with OCT at implantation, IVUS and OCT were compared at the time of explantation by means of stent area, strut number, strut thickness and mean lumen diameter.

The stent area comparison was performed by matching results from pairs of 77 cross-sections. There was a significant ($p<0.01$) yet moderate correlation between the two methods ($r=0.36$). The AMS stent area measured by OCT was smaller than IVUS, while the BMS stent area was larger (Figure 21A, B, C).

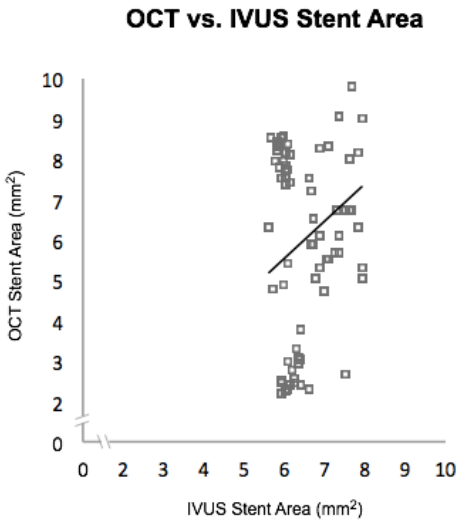

Figure 21A: Comparison of stent area as measured with IVUS and OCT. There was a significant ($p<0.001$) yet moderate correlation between the two methods ($r=0.35$).

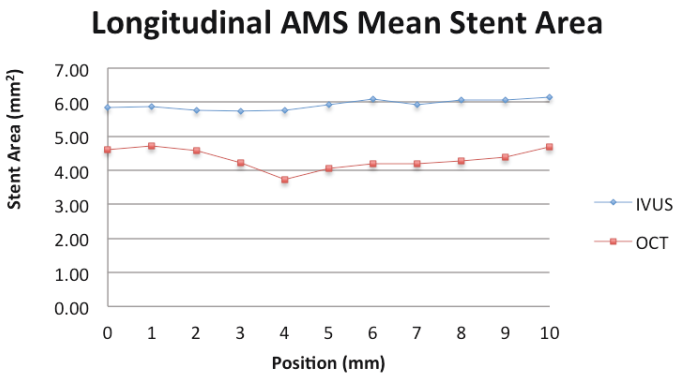

Figure 21B: Longitudinal comparison of AMS stent area as measured by IVUS and OCT. OCT measured a consistently smaller stent area for AMS.

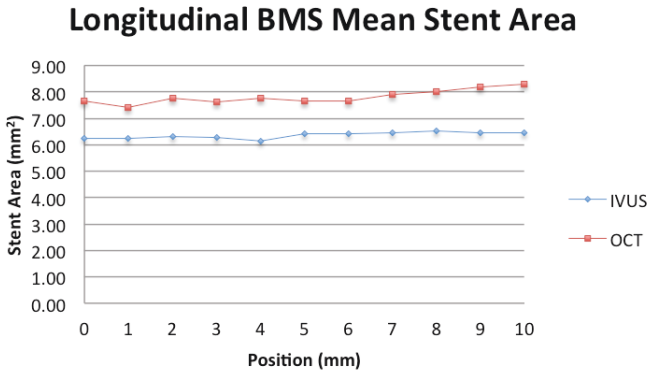

Figure 21C: Longitudinal comparison of BMS stent area measured by IVUS and OCT. OCT measured a consistently larger stent area for BMS.

For the strut number comparison, measurements from 71 cross-sectional pairs of IVUS and OCT were used. For IVUS the mean strut number was 6.5±2.97, while for OCT this number was 6.07±2.20. The strut number varied due to the changing angle of the visualization of the cross-section, and therefore there is no correlation for this number between IVUS and OCT. The results, however, do point to OCT being able to visualize a larger number of AMS struts, but a smaller number of BMS struts (Figure 22A, B).

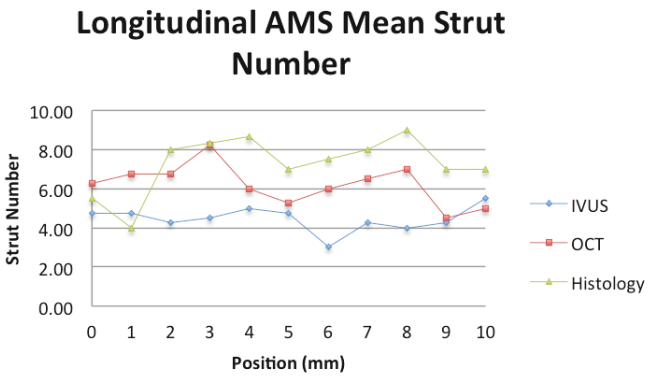

Figure 22A: Longitudinal comparison of IVUS, OCT and histology by means of strut number. There was no significant correlation between these methods, though histology tended to capture more AMS struts than OCT, followed by IVUS.

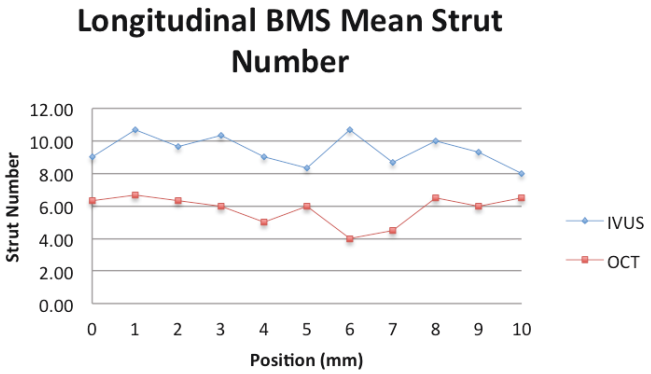

Figure 22B: Longitudinal comparison of IVUS and OCT by means of BMS strut number. There was no significant correlation between these methods, though IVUS tended to capture more BMS struts.

Next, strut thickness was compared between 71 pairs of cross-sections. Results show that there is a negative moderate correlation between IVUS and OCT ($r=-0.46$, $p<0.01$), which indicates that the thicker a strut appears in IVUS, the thinner it is in OCT. The strut thickness for OCT was found to be smaller than the strut thickness for IVUS for both AMS and BMS (Figure 23A, B).

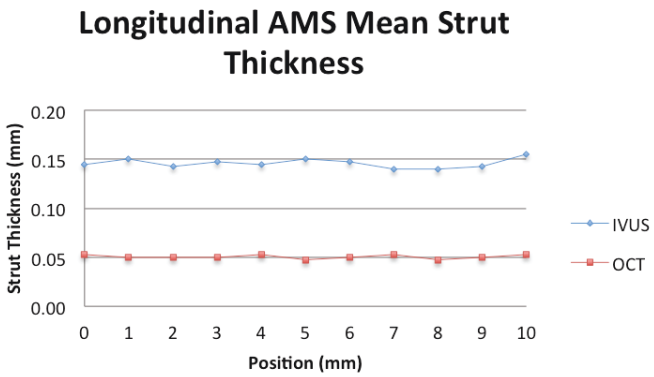

Figure 23A: Longitudinal comparison of IVUS and OCT by means of AMS strut thickness. The OCT strut thickness was consistently smaller than that measured by IVUS.

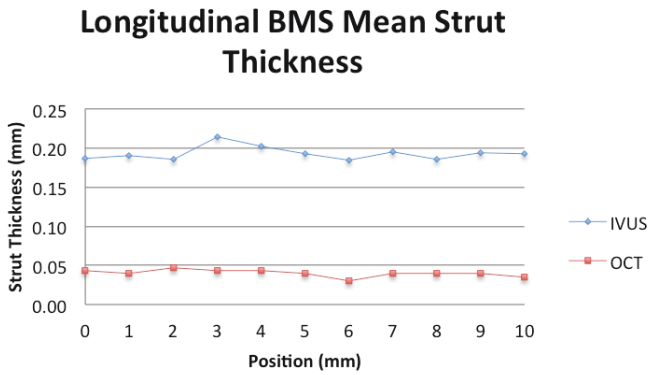

Figure 23B: Longitudinal comparison of IVUS and OCT by means of BMS strut thickness. The OCT strut thickness was consistently smaller than that measured by IVUS.

For comparison of mean lumen diameter, 73 pairs of cross-sections were used. There was a significant and moderate correlation between IVUS and OCT ($r=0.36$, $p<0.01$). The mean lumen diameter for OCT was smaller than that of IVUS (Figure 24A, B, C).

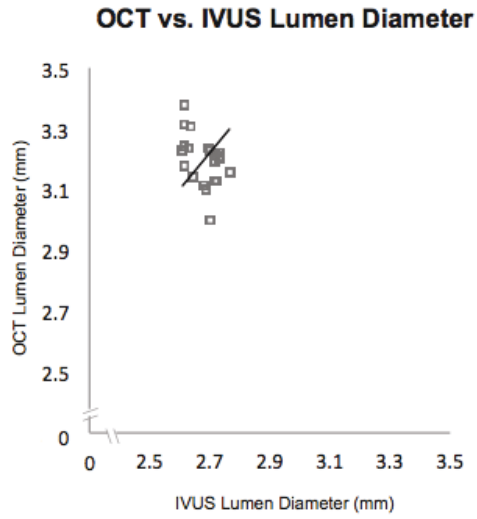

Figure 24A: Comparison of OCT vs. IVUS by means of mean lumen diameter. There was a significant and moderate correlation between the two methods ($r=0.36$, $p<0.01$).

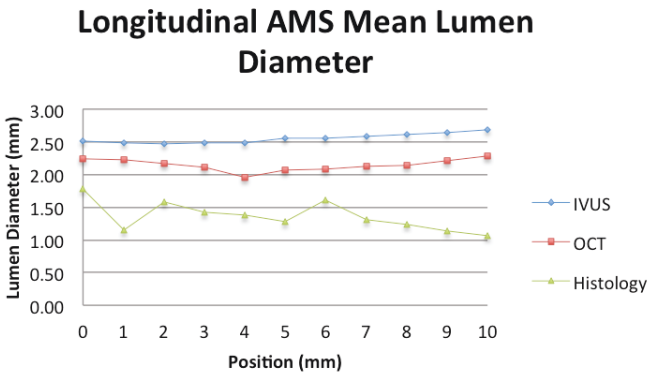

Figure 24B: Longitudinal comparison of IVUS, OCT and histology by means of AMS lumen diameter. The mean lumen diameter for OCT and histology was smaller than that of IVUS (IVUS>OCT>histology).

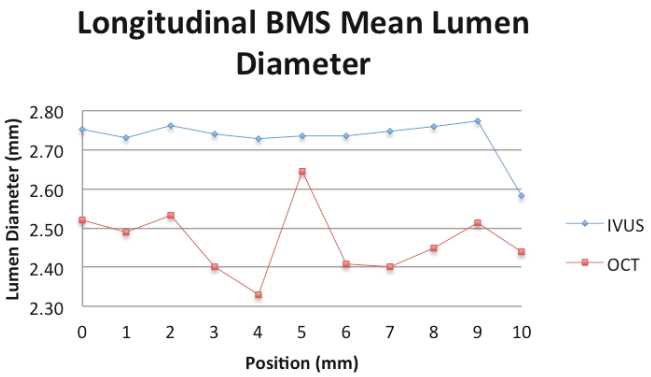

Figure 24C: Longitudinal comparison of IVUS and OCT by means BMS lumen diameter. The mean lumen diameter for OCT was smaller than that of IVUS.

IVUS and OCT (in-vivo) vs. Histology (ex-vivo)

Histology offered a highly detailed assessment of the AMS-stented coronary vessels. Not only was a three-layered vessel wall able to be visualized thanks to Movat's pentachrome staining, but it also helped us assess and understand the discrepancy between IVUS and OCT by displaying neointima and thrombus formations (Figure 25, 26).

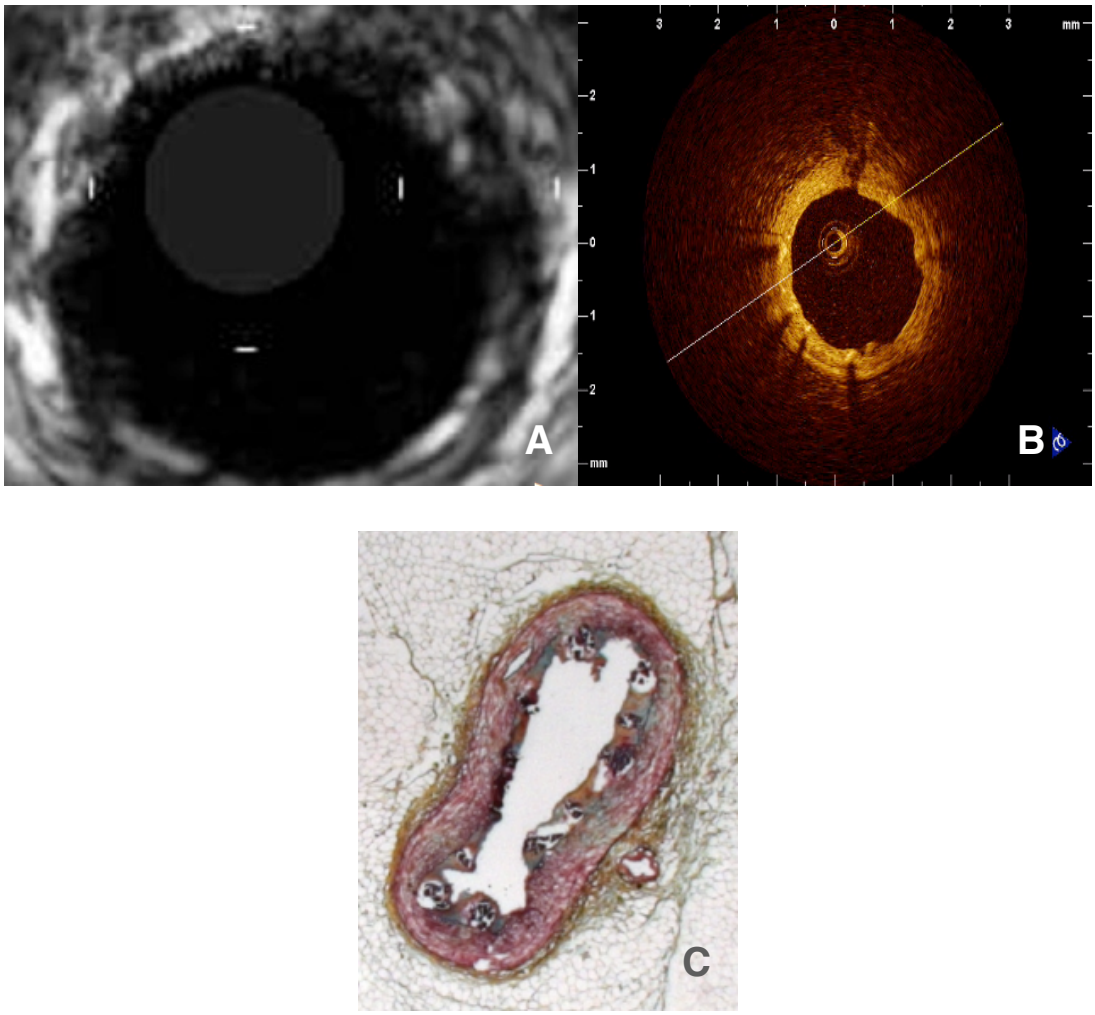

Figure 25A, B, C: Comparison of in-vivo (A: IVUS, B: OCT) and ex-vivo (C: Histology with MPS) degradation visualization. While the in-vivo methods captured the biodegradation as a reduction of signal intensity of the AMS struts, the ex-vivo technique provided valuable information about the morphology of this degradation process.

This comparison was only performed on AMS. Both the strut number and mean lumen area were compared with 19 pairs of cross-sections.

While IVUS captured 4.45±1.47 struts, OCT captured 6.20±2.1, and histology captured 7.53±2.17. Due to changes in stent geometry as a function of the location of the cross-section, there was again no correlation between these three methods by

means of strut number. Histology captured a larger strut number than OCT and IVUS (Figure 22A).

There was no significant correlation for the mean lumen diameter between IVUS and histology. However, comparison of the mean lumen diameter between OCT and histology showed a significant and moderate correlation ($r=0.74$, $p<0.01$, see Figure 25). IVUS tended to measure larger lumen diameters than OCT and histology (IVUS>OCT>histology, see Figure 24B).

While comparing the three methods, it was interesting to see that IVUS consistently missed the neointima formation that was captured in both OCT and histology (Figure 25). This finding helps us to understand the outliers of different method that possibly reduce the correlation.

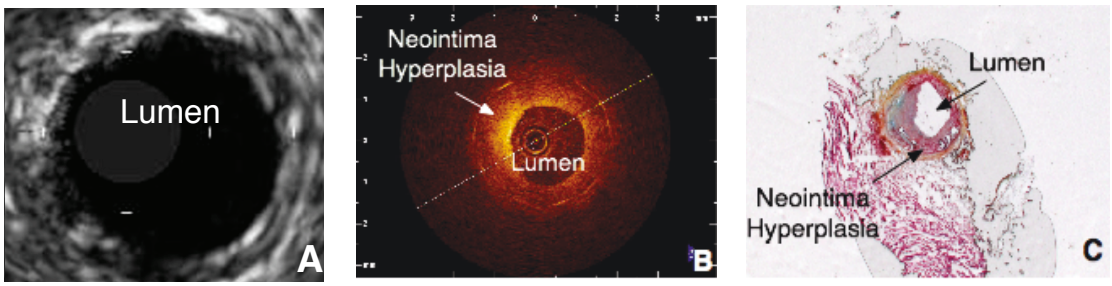

Figure 26: OCT (B) displayed a smaller lumen diameter in comparison to IVUS (A). As can be seen with histology (C), the lumen of this vessel was narrowed by an eccentric tissue proliferation consistent with neointima hyperplasia, which reinforced OCT's assessment of the vessel.

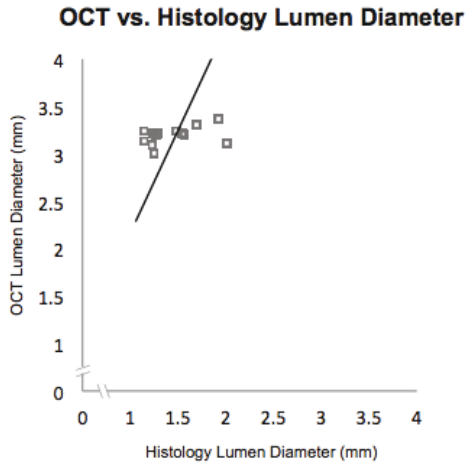

Figure 27: Comparison of histology and OCT by means of lumen diameter. This study showed a significant and moderate correlation between these two methods ($r=0.74$, $p<0.01$).

Assessment of Staining on Histological Morphometry

Native vs. Stained Vessel Segment Comparison

42 cross-sections were chosen at random, while 14 of them were destroyed during sample preparation (during cryosectioning, mounting, or staining) so that only 28 cross-sections were left. 22 out of these 28 cross-sections contained AMS stented vessels, while the rest were reference segments without any stent implantation.

Movat's pentachrome was chosen as the stain and the properties of interest of the cross-sections were their: lumen area, intima area, vessel area, minimum and maximum lumen diameter, as well as their strut number and strut area.

There was no noticeable size difference between the native and stained segments. In comparison to the images acquired with IVUS and OCT, the vessels were in an oval shape. One potential cause for this may have been the embedding process. All three layers of the vessel could be identified for both the native and stained cross-sections. Their internal elastic lamina (IEL) and external elastic lamina (EEL) appeared black in both methods, as did the stent struts, which were covered with a thin endothelial lining colored in red from the staining (Figure 28A, B).

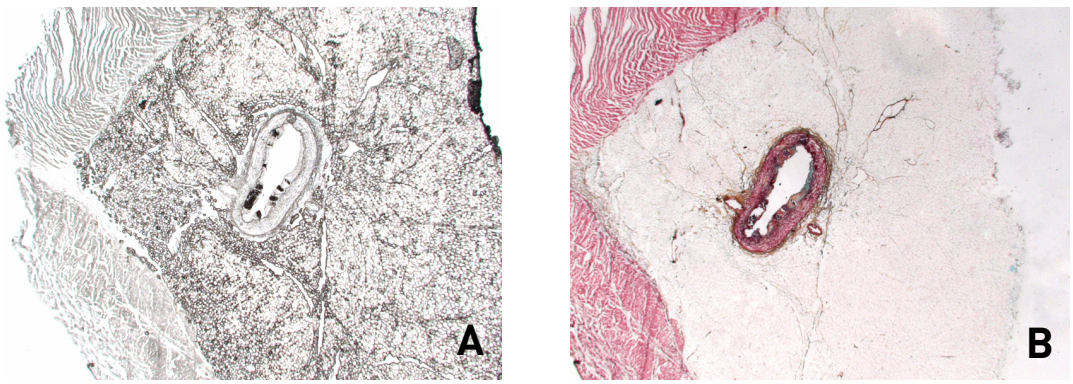

Figure 28: Comparison of native (A) and MPS (B) cross-sections of an AMS-stented segment. All three layers of the vessel could be identified for both the native and stained cross-sections. Their internal elastic lamina (IEL) and external elastic lamina (EEL) appeared black in both, as did the stent struts, which were covered with a thin endothelial lining colored in red from the staining. Furthermore, it was apparent that some struts were washed out during the staining and missing from the stained segments.

Lumen Area

The lumen area for the native cross-sections had a mean of 1.34±0.35 mm^2 (range: 0.75-2.10 mm^2). The stained cross-sections had a lumen area with a mean of 1.27±0.36 mm^2 (range: 0.69-2.04 mm^2). Neither group had a significant difference (p

< 0.01) and their correlation was strong (r = 0.975) (Figure 29).

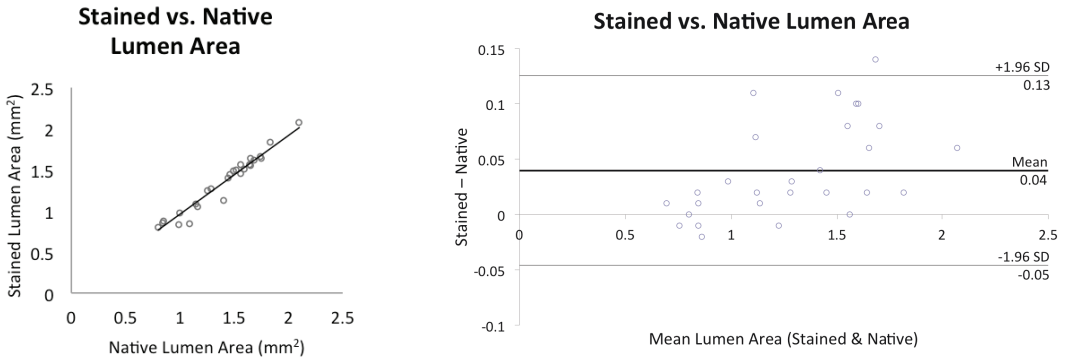

Figure 29: Comparison of native and MPS cross-section by means of the lumen area. Neither group had a significant difference (p < 0.01) and their correlation was strong (r = 0.975).

Intima Area

The mean intima area for the native cross-sections was 2.20±0.78 mm^2 (range: 1.31-4.21 mm^2) The stained intima area was meanwhile measured as 2.21±0.76 mm^2 (range: 1.28-4.23 mm^2). The results also correlate strongly (r=0.975) and display no significant difference (p<0.01) (Figure 30).

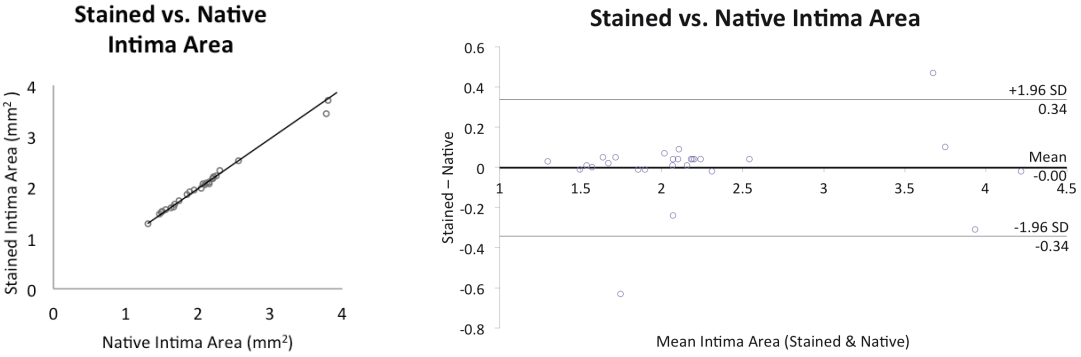

Figure 30: Comparison of native and MPS cross-sections by means of intima area. These results also correlate strongly (r=0.975) and display no significant difference (p<0.01).

Vessel Area

The vessel area for the native cohort turned out to be 3.5±0.72 mm^2 (range: 2.45-5.14 mm^2). For the stained group, the mean vessel area was determined to be 3.58±0.75 mm^2 (range: 2.50-5.68 mm^2). Again, there was no significant difference between groups (p<0.01) and they correlated strongly (r=0.98) (Figure 31).

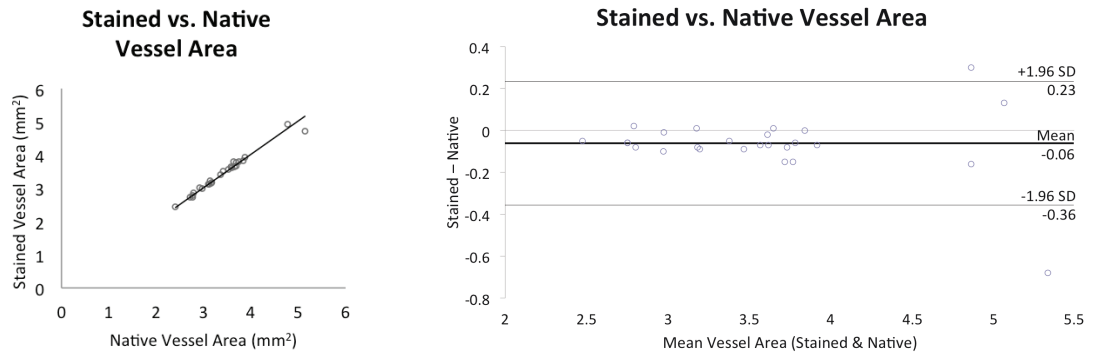

Figure 31: Comparison of native and MPS cross-sections by means of the vessel area. There was no significant difference between groups ($p<0.01$) and they correlated strongly ($r=0.98$)

Maximum Lumen Diameter

In order to calculate the maximum lumen diameter, the visually largest diameter was chosen. The mean maximum lumen diameter was 1.75±0.27 mm (range: 1.27-2.32 mm). For the stained cohort, their mean was 1.75±0.29 mm (range: 1.10-2.32 mm). There was no significant difference ($p<0.01$) and both methods correlated very well ($r=0.918$) (Figure 32).

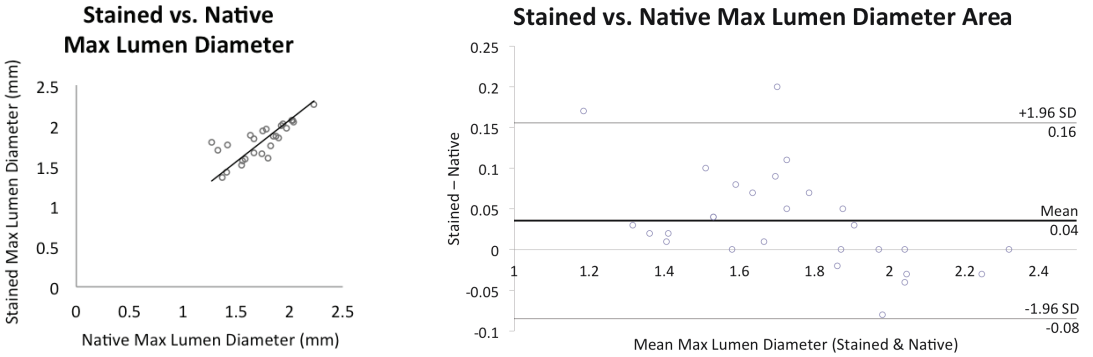

Figure 32: Comparison of native and MPS cross-sections by means of the maximum lumen diameter. There was no significant difference ($p<0,01$) and both methods correlated very well ($r=0.918$).

Minimum Lumen Diameter

The minimum lumen diameter was also determined by visual inspection. The mean value for the native group was 0.90±0.31 mm (range: 0.35-1.42 mm). The stained segments had a mean of 0.85±0.31 mm (range: 0.038-1.42 mm). There was no significant difference ($p<0.01$) and a strong correlation ($r=0.923$) between the two methods (Figure 33).

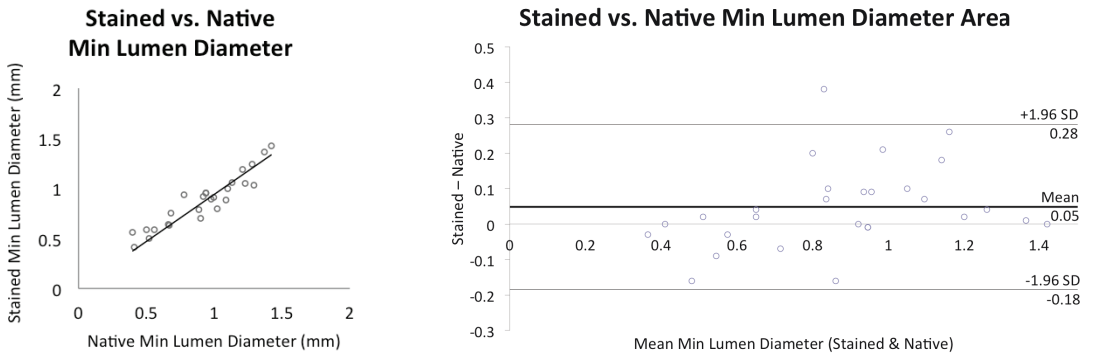

Figure 33: Comparison of native and MPS cross-sections by means of the minimum lumen diameter. There was no significant difference ($p<0.01$) and a strong correlation ($r=0.923$) between the two methods.

Strut Number

For the native cohort, there was a mean strut number of 8.18±2.78 (range: 3-25). The mean strut number for the stained group was 6.95±3.06 (range: 5-14). The methods possessed no significant difference ($p<0.01$) and a moderate correlation ($r=0.86$)(Figure 34).

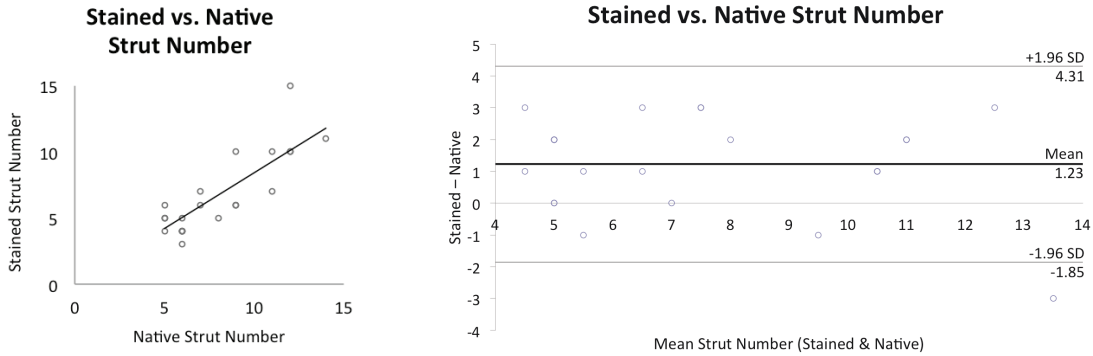

Figure 34: Comparison of native and MPS cross-sections by means of the strut number. The methods possessed no significant difference ($p<0.01$) and a moderate correlation ($r=0.86$)

Strut Area

In order to determine strut area for each cohort, every single strut within a cross-section was plotted and averaged. For the native group, the mean strut area was 0.04±0.01 mm^2 (range: 0.02-0.08 mm^2). For AMS, the mean strut area was 0.03±0.01 mm^2 (range: 0.02-0.06 mm^2) for the stained group. The charts below illustrate no significant difference ($p<0.01$) and only a moderate correlation $r=0.565$ (Figure 35). The moderate correlation is most likely due to the fact that during cryosectioning some struts cracked and were partially washed away during staining (Figure 36).

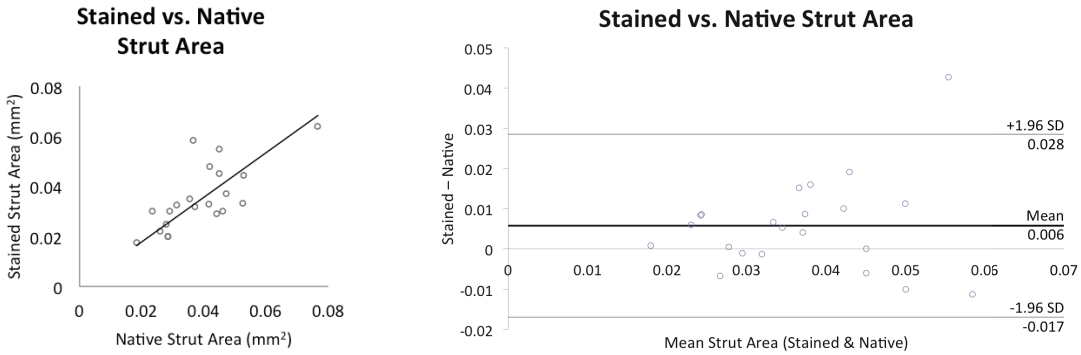

Figure 35: Comparison of native and MPS cross-sections by means of the strut area. The charts illustrate no significant difference ($p<0.01$) and only a moderate correlation $r=0.565$.

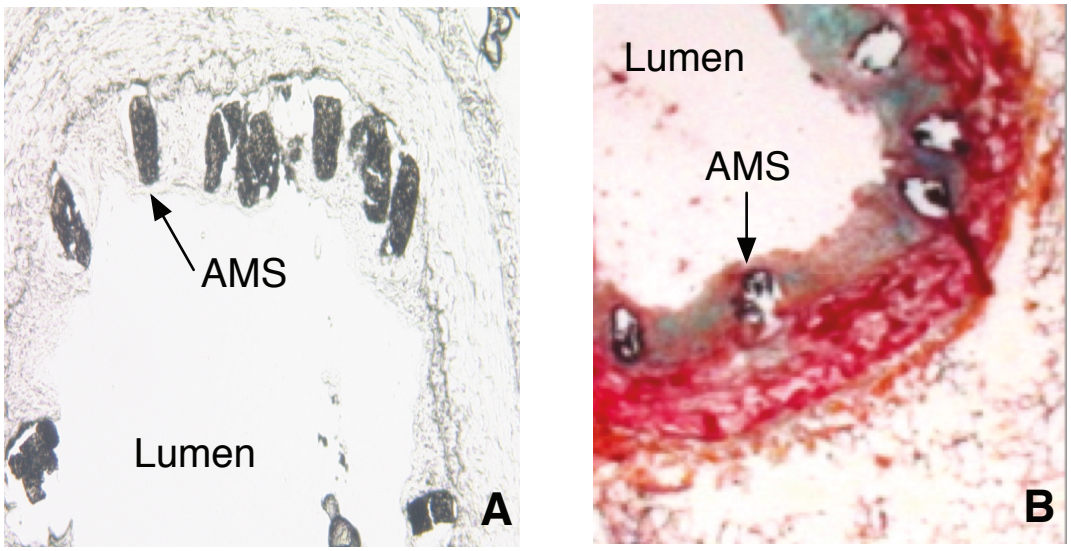

Figure 36A, B: As can be seen in the image of the native cross-section (A), during cryosectioning some struts cracked and therefore during staining were partially washed away, as can be seen in the stained cross-section (B).

Intra-observer Reproducibility

To determine intra-observer reproducibility, the morphometry of the stained samples (the same ones from the comparison of native vs. stained study) was repeated three months later. Overall, the comparison showed an excellent significant correlation consistent with high intra-observer reproducibility. The calculated correlation for each different parameter was as followed: lumen area ($\kappa=0.99$, $p<0.01$), intima area ($\kappa=0.98$, $p<0.01$), media area ($\kappa=0.99$, $p<0.01$), maximum diameter ($\kappa=0.99$, $p<0.01$), minimum diameter ($\kappa=0.99$, $p<0.01$), strut number ($\kappa=0.99$, $p<0.01$). Only the strut area showed a moderate correlation ($\kappa=0.75$, $p<0.01$).

Discussion

Animals, Safety and Feasibility

Due to the similarity of their cardiovascular system to our own, Gottingen minipigs were chosen as subjects for this study[71]. One significant difference between the physiology of the heart of Gottingen minipigs and the human heart is their vulnerability to arrhythmia. During OCT acquisition, two out of the four minipigs had to be defibrillated after developing ventricular tachycardia due to ischemia in the examined area caused by the balloon occlusion.

With IVUS, almost all vessels could be properly visualized. Only at time of explantation could one vessel not be examined because the guiding catheter was unable to pass the in-stent stenosis. Similar to other studies[26, 31], there were no complications during this study. IVUS delivered a consistently high image quality, and as no complications occurred during image acquisition at time of implantation or explantation, the conditions were optimal while these vessels were visualized with this technique.

Visualization with OCT was markedly more complicated. One vessel was dissected and occluded at time of implantation, so it was not possible to study this vessel later at the time of explantation. Though two animals developed ventricular fibrillation during occlusion at the time of implantation (only one of them could be successfully defibrillated), no arrhythmia complications occurred during explantation and all vessels but one could be visualized (the same vessel that could not be visualized with IVUS). One reason that no arrhythmia complications occurred at the time of explantation and only at implantation may be that the stent implantation and IVUS acquisition led to a spasmogen stimulus in the vessel – an effect missing at the time of explantation. In contrast to our own findings, Yamaguchi et al showed that while the occlusion technique in clinical settings led more frequently to transient events such as chest discomfort no major or acute procedural complications were observed[82]. Since OCT acquisition for this study was performed on healthy non-atherosclerotic vessels rather than the atherosclerotic vessels used in Yamaguchi's study, it's possible that these were more sensitive to spasmogen stimulus. And finally, since Kataiwa et al also demonstrated that in a comparison of non-occlusive and occlusive imaging

techniques for a small patient cohort (n=40) that the non-occlusive technique was safer[42], for further research the non-occlusive method should be the preferred technique. It should also be noted that an animal model cannot be applied to humans without restrictions.

The quantitative analysis with OCT was also more difficult than with IVUS. Due to the limited penetration depth of OCT, vessels with large lumens or thick walls could not be adequately assessed. Additionally, due to the sensitivity of its catheter tip, a consistently high image quality was not possible. Therefore not all the vessels visualized with the OCT could be assessed for vessel morphometry. So few were the number of samples at the time of implantation that no comparison could be made between implantation and explantation.

While IVUS and OCT were used to visualize both AMS and BMS, histology was only performed on AMS due to the technical difficulties mentioned earlier. And since a few samples were destroyed during the preparation, this further reduced the number of cross-sections available to study

Comparison of IVUS, OCT, and Histology

Quantitative Assessment

Histology offered a detailed assessment of the three-layered vessel anatomy and was also able to detect thrombus and neointima formation, as well as stent endothelization. Thanks to its high resolution, OCT clearly visualized the lumen-intima interface as a sharply defined border, and also clearly captured the neointima formation, stent endothelization and stent malapposition[6, 9]. OCT provides such a detailed assessment of tissue near struts because the light is unable to penetrate the struts, leading to weak signal reflections from struts, thus facilitating imaging[46]. IVUS, however, tended to miss these details since the ultrasound waves that are reflected from the struts interfere with those reflected from the surrounding tissue, resulting in the tissue around the struts not able to be properly visualized[49].

Both IVUS and OCT were able to visualize the biodegradation. A signal reduction of AMS struts was apparent in both methods. Inline with the Slottow et al findings[61], the AMS struts appeared more diffuse and had less discernible distal acoustic shadowing

with OCT. At the time of explantation, IVUS presented AMS struts as poorly defined echolucent areas. Similar results were also observed in some other studies[16, 23, 24, 80, 61]. No change was detected for BMS with either technique.

Vessel Morphometry

Due to its consistently high image quality, IVUS was the only method that reliably visualized the stented coronary vessels along their whole length both at the time of implantation and explantation. Therefore IVUS was the only in-vivo technique available to us to compare stent dimensions acquired over the four weeks. It captured the biodegradation process as an overall reduction in stent area, strut number, strut thickness and lumen diameter for AMS, while there was no change detected in the BMS.

Compared to OCT and histology, IVUS tended to overestimate AMS-stented vessel dimensions. Similar results, especially with respect to lumen area, were also shown by Suziki et al[72] and Kawase et al[43]. This overestimation could be attributed to the difficulty in clearly identifying the lumen border in IVUS images due to blood speckle[28], or the presence of artifacts such as side lobes (extraneous beams of ultrasound generated from the edges of individual transducer elements that are not in the direction of the main ultrasonic beam) that result from strut reflections[49]. The differing catheter diameters of the IVUS (1 mm) and OCT (0.4 mm) are also potential culprits.

IVUS and OCT showed a moderate to good correlation by means of stent area, strut thickness and mean lumen diameter. One reason for the moderate correlation could be the different slice thicknesses of both methods (20 μm for OCT and 300 μm for IVUS), and the movement of the catheter in the beating heart that causes a variability of dimensions. Previous studies have shown that IVUS tends to overestimate larger vessels and underestimate the smaller ones[68], though another explanation could be the calibration of the sensitive OCT catheter during image acquisition can affect the results. Some outliers – like vessels with neointima formations – led to extreme variation between the techniques because the resulting morphology change was detected by OCT and histology, but not by IVUS. This helps to understand why IVUS and histology did not correlate by means of lumen diameter, while OCT and histology did.

The strut number varied so highly between techniques likely due to the changing cross-sectional visualization angle and different slice thicknesses between techniques: IVUS (300 μm) > OCT (20 μm) > Histology (10 μm). This resulted in no correlation for strut number between any of the methods. Correlation aside, the longitudinal comparison did demonstrate that histology was able to capture more struts than OCT and IVUS (Histology>OCT>IVUS). One possible reason for IVUS capturing fewer struts may be due to a weaker reflection of the ultrasound from AMS. Thus, the echogenicity was slightly lower and clearly identifying AMS struts was at times difficult. It is also possible that IVUS underestimated the stent area due to this same limitation.

Titan Yellow Stain

The two existing in-vitro (the immersion and electrochemical tests) and in-vivo (IVUS and OCT) methods commonly used to study the biodegradation of magnesium stents are not able to capture the distribution of magnesium within the vessel. In order to capture this degradation pattern in a real-life setting we needed to identify a staining method that would selectively visualize magnesium. Due to its employment in previous successful studies and ease of use, we chose to work with titan yellow. The main limitation of staining AMS-stented vessels is that, as a biodegradable metal, the AMS might dissolve in the aqueous environment. For this reason we modified the titan yellow staining procedure to minimize the stents' exposure to water and alcohol. This experiment helped us to selectively visualize the AMS struts and capture their degradation products diffusing into the surrounding tissue. This was the first study to show that biodegradable magnesium stents and their degradation products can be visualized in an ex-vivo study, which in turns allows us to use these images to compare and better understand the changes due to degradation during in-vivo visualization. The simplicity and speed of the titan yellow staining procedure also puts it at a large advantage over the in-vitro corrosion techniques previously employed.

The only drawback to the titan yellow staining technique faced during this study was its decreased effectiveness of the staining procedure over time. This is an issue that should be investigated as the topic of another study.

Assessment of Staining on Histological Morphometry

Overall there was a significant correlation between native and stained cross-sections by means of lumen area, intima area, vessel area, maximum and minimum lumen diameter. In 1985 Siegel et al demonstrated that histological preparation changed the vessel dimensions of atherosclerotic coronary vessels based on the extent of the atherosclerosis[69]. For vessels with minimal atherosclerotic narrowing, histological preparation decreased the total vessel and lumen cross-sectional areas, whereas it did not affect the absolute wall area. In contrast, for vessels with moderate to severe atherosclerosis, histological preparation decreased both the wall area and total cross-sectional area while the lumen cross-sectional area stayed the same. The discrepancy between this study's findings and those by Siegel et al can be explained by the differing subjects (in this study the vessels were stented and otherwise healthy) and methods of histological preparation (both staining and fixation methods differed) [17]. Siegel et al used atherosclerotic coronary vessels and fixed them with formalin, so this set of results can complete each other.

The comparison of native and stained cross-sections showed a moderate correlation by means of strut number and strut area. During cryosectioning some struts cracked and therefore during staining were partially washed away. While some examiners might be led to believe that a reduction in strut number and area is a clear indication of biodegradation, it's in fact just a result of the staining process itself. Histology showed overall a very high intra-observer reproducibility. The only exception to this was the strut number, which showed a moderate correlation most likely due to the difficulty in determining the borders of individual struts after staining (caused by the wash-out effect).

Conclusion

Biodegradable magnesium alloy stents (AMS) are a new and promising advancement in interventional cardiology. The human body absorbs these stents once they have served their mechanical purpose (temporary scaffolding) after about 2-3 months, allowing AMS to circumvent the existing adverse effects of stenting (such as late thrombosis, in-stent stenosis) and restore vasomotion. Now, with the aid of recent innovations (e.g. drug eluting absorbable metal stents), these stents may set a new standard for coronary stenting.

The aim of this study was twofold: to study the available in-vivo visualization techniques (OCT and IVUS) in order to identify their strengths and weaknesses in assessing the biodegradation process of AMS better and compare those findings with histology, and secondly to identify a new histological technique to study the distribution of magnesium and its degradation products in to surrounding tissue upon biodegradation.

Both IVUS and OCT are effective in-vivo visualization techniques to study the biodegradation process of AMS. IVUS is superior to OCT in capturing vessel morphometry thanks to its ease of use and consistently high image quality, thus enabling us to study the vessel dimensions during biodegradation. OCT, however, is a better technique for detailed vessel assessment thanks to its higher resolution, and helps us to detect the qualitative changes during biodegradation. Thanks to recent improvements in OCT (esp. non-occlusive techniques), better quantitative visualization with OCT can now be expected.

Both in-vivo methods (OCT and IVUS) showed a moderate correlation. The histological studies showed a poorer correlation with these in-vivo techniques; measurements were consistently largest with IVUS and smallest with histology (IVUS > OCT > histology). Staining did not affect most stent measurements, and the reduction in strut number and area was likely due to the strut integrity compromised by cryosectioning and struts subsequently washed away during staining. As this effect could cause confusion in serial histology studies observing biodegradation, it is important to determine the washout effect of staining on struts for future studies.

Though IVUS and OCT together offer a gross understanding of AMS biodegradation, in order to complete this view at a cellular level one must employ a third technique. The technique investigated in this study was titan yellow staining, which proved to be a feasible method for capturing the biodegradation process and the distribution of magnesium within the vessel wall. This study showed for the first time that biodegradable magnesium stents and their degradation products can be visualized effectively ex-vivo, and analysis from these images will allow us to better understand changes due to degradation during in-vivo visualization. Its simplicity and speed make titan yellow preferred to the in-vitro corrosion techniques previously employed. The procedure, however, must be further modified in order to improve its effectiveness over a longer period of time. Once this is achieved, it will then be possible to measure the density of degradation products away from struts over time, so as to more thoroughly understand the degradation kinetics.

Abstract

Percutaneous coronary intervention (PCI) is the most common treatment for coronary artery disease (CAD). The first form of PCI introduced was balloon angioplasty. After that, the advent of coronary stents (tubular wire mesh for intravascular mechanical support) led to a new era in interventional cardiology. Through the implantation of bare metal stents (BMS), all three limitations of balloon angioplasty – coronary artery dissection, elastic recoil and negative remodelling – are prevented. Unfortunately, bare metal stents have their own drawbacks: most significantly, in-stent stenosis as a result of deep focal vascular injury caused by stent struts, followed by excessive tissue proliferation. This drawback has since been addressed with the introduction of drug eluting stents (DES).

Both BMS and DES are permanent stents. As foreign bodies implanted into coronary vessels, they cause the following adverse effects: hypersensitivity reaction, chronic inflammation, elimination of vasomotion, and stent thrombosis.

Biodegradable stents have been set forth as a candidate to overcome the drawbacks of permanent stents through providing temporary mechanical stability for a vulnerable lesion before complete degradation without long-term impairment of vessel function. The two main materials used in biodegradable stents are poly-L-lactide and metal (or AMS, short for absorbable metal stents). One type of AMS is magnesium alloy.

Before AMS become a standard in the treatment of CAD, more research is required to better understand their degradation kinetics and mechanical stability. In order to complete these studies, however, the stents must provide adequate opacity for visualization – wherein lies the challenge. It is not possible to visualize magnesium stents with coronary angiography. Newer imaging modalities such as optical coherence tomography (OCT) and intravascular ultrasound (IVUS) have been proposed as techniques to visualize these stents and their biodegradation.

The aim of this study was twofold: first, to study the available in-vivo visualization techniques (OCT and IVUS) in order to identify their strengths and weaknesses in assessing the biodegradation process of AMS through comparison with histology; and

secondly, to identify a new histological technique for studying the distribution of magnesium and its degradation products into surrounding tissue upon biodegradation.

Four Gottingen mini pigs were implanted with AMS and BMS, and assessed with IVUS and OCT under fluoroscopic guidance at the time of implantation and prior to explantation (4 weeks later). Upon completion of the in-vivo studies, the hearts of the study objects were harvested for histological processing.

Results showed that both IVUS and OCT are effective visualization techniques in studying the biodegradation process of AMS. IVUS is superior to OCT in capturing vessel morphometry thanks to its ease of use and consistently high image quality, thus enabling us to study vessel dimensions during biodegradation. OCT, however, is a better technique for detailed vessel assessment thanks to its higher resolution, and helps us to detect qualitative changes during biodegradation. The two methods correlate moderately during the morphometric analysis. The histological studies on the other hand showed a poorer correlation with the in-vivo techniques. This was likely due to strut integrity compromised during cryosectioning and subsequently washed away after staining, as in an adjunctive study we were able to show that staining did not affect morphometry. The measurements were consistently largest with IVUS, and the smallest with histology (IVUS > OCT > histology).

Though IVUS and OCT together offer a gross understanding of AMS biodegradation, in order to complete this view at a cellular level one must employ a third technique. The technique investigated in this study was titan yellow staining, which proved to be a feasible method for capturing the biodegradation process and the distribution of magnesium within the vessel wall. This study showed for the first time that biodegradable magnesium stents and their degradation products can be visualized effectively ex-vivo, and that analysis of these images will allow us to better understand the changes due to degradation during in-vivo visualization. Its simplicity and speed make titan yellow preferred to the in-vitro corrosion techniques previously employed. The procedure, however, must be further modified in order to improve its effectiveness over a longer period of time. Once this is achieved, it will then be possible to measure the density of degradation products away from struts over time, so as to more thoroughly understand the degradation kinetics.

Zusammenfassung

Die perkutane koronare Intervention (PCI, percutaneous coronary intervention) ist heute die Standardtherapie zur Behandlung der koronaren Herzerkrankung. War es in der Anfangszeit der PCI die alleinige Ballondilatation, so hat sich in den Folgejahren durch die Entwicklung von koronaren Stützprothesen (Stents) das Einsatzspektrum und die Anwendungssicherheit deutlich vergrößert. Durch die Einführung der Stents konnte Problemen wie der lumenobstruierende Dissektion sowie den elastischen Rückstellkräften (elastic recoil) wirkungsvoll begegnet werden. Ein wesentliches Problem dieser frühen Stentgenerationen war jedoch das Auftreten von Restenosen im Bereich der Stents, die im Wesentlichen durch ein überschiessendes Wachstum von Endothel- und glatten Muskelzellen bedingt waren. Um diesem Problem zu begegnen, wurden verschiedene Verfahren eingesetzt, von denen sich heute jedoch nur die Beschichtung der Stents mit proliferationshemmenden Substanzen (sog. drug eluting stents = DES) durchgesetzt hat.

Ein wesentliches systemimmanentes Problem dieser Stents ist jedoch, dass durch die Stentimplantation Fremdmaterial permanent in die Koronargefäße eingebracht wird, das die Physiologie der Gefäßwand verändert und so z.B. zu chronischen Inflammationsreaktionen oder dem Auftreten von Thrombosen führen kann.

Der Entwicklung von sog. biodegradierbaren Stents liegt daher die Überlegung zu Grunde, eine Technik bereitzustellen, die in der akuten Situation die mechanischen Vorteile von konventionellen Stents bietet und sich nach Behebung der akuten Situation, bzw. der Umwandlung einer „vulnerablen Läsion“ in eine stabile Läsion idealerweise rückstandsfrei auflöst.

Um diese Eigenschaften zu erreichen, werden heute entweder Materialien auf Milchsäurebasis oder bestimmte Metalllegierungen (absorbable metal stents= AMS) auf Magnesiumbasis verwandt.

Bei der Weiterentwicklung und Verbesserung dieser biodegradierbaren Stents kommt der koronaren Bildgebung eine wesentliche Rolle zu. Hiermit lassen sich wesentliche Eigenschaften der Stents während des Degradationsprozesses untersuchen. Die konventionelle Röntgendarstellung (Angiographie) ist aufgrund der geringen

Schwächung durch Magnesium oder auch Milchsäurederivate von untergeordneter Bedeutung.

Statt dessen kommen hier vorallem neuere intrakoronare Bildgebungsmethoden wie intravaskulärer Ultraschall (IVUS) oder die optische Kohärenztomographie(OCT) zum Einsatz.

Ziel der vorliegenden Arbeit war es , die Abbildungseigenschaften von IVUS und OCT beim Degradationsprozess zu untersuchen und die erhaltenen Ergebnisse mit der histologischen Untersuchung zu vergleichen. Ausserdem sollte nach einer Möglichkeit gesucht werden, die Verteilung von Magnesium in der Gefäßwand, die im Rahmen des Degradationsprozesses stattfindet, mit histologischen Verfahren sichtbar zu machen. Für die experimentellen Untersuchungen am Tiermodell wurden insgesamt zehn AMS und BMS in vier Göttinger Minischweine implantiert und die Gefäße mittels IVUS und OCT bei Implantation und nach vier Wochen dargestellt. Anschließend erfolgte die histologische Evaluierung.

Als ein wesentliches Ergebnis der Arbeit konnte gefunden werden, dass IVUS, wie auch OCT geeignet waren, den Prozess der Biodegradation darzustellen Bezüglich der Sicherheit und der Einfachheit der Anwendung war jedoch IVUS dem OCT deutlich überlegen. Im Gegenzug konnte mithilfe des OCT die Stentgeometrie, die Dicke der Neointima und auch Thrombusbildung sehr genau dargestellt werden. Beim Vergleich der beiden Methoden bezüglich der morphometrischen Stentanalyse konnte eine sehr hohe Übereinstimmung gefunden werden. Der Vergleich mit der nach Explantation durchgeführten Histologie lieferte bezüglich der quantitativen Parameter aber deutlich unterschiedliche Werte. Der Grund hierfür ist sicherlich in der komplizierten histologischen Aufarbeiten zu suchen, wenngleich ein substantieller Einfluß der eigentlichen Färbung durch eine dezidierte Substudie ausgeschlossen werden konnte.

In der Tendenz lieferte der IVUS für die Gefäß- und Stentdimensionen im Schnitt die größten Werte, gefolgt von der OCT. Die morphometrische Analyse der histologischen Präparate ergab in der Regel die kleinsten Werte.

Neben der morphometrischen Analyse war ein wesentlicher Aspekt der Arbeit der Versuch, die Abbauprodukte der AMS (im Wesentlichen elementares Magnesium) in ihrer Verteilung zu untersuchen. Hierzu wurde eine Modifikation einer Färbung nach

Kolthoff (Titan Gelb Färbung) entwickelt und an den vorliegenden Präparaten etabliert.

Hierdurch konnte sehr schön die Deposition des elementaren Magnesiums in der näheren Umgebung der Stentstreben in der Gefäßwand nachgewiesen werden.

Gleichwohl ist die Färbemethode in ihrer derzeitigen Anwendung nicht langzeitstabil und unterliegt noch größeren Schwankungen. Hier sind umfangreichere Studien notwendig um die diese Färbetechnik noch besser zu standardisieren und ggf. neben einer qualitativen Aussage auch noch eine quantitative Analyse der Magnesiumablagerung zu erhalten.

Bibliography

1. ASTM International. ASTM F2129: Standard Test Method for Conducting Cyclic Potentiodynamic Polarization Measurements to Determine the Corrosion Susceptibility of Small Implant Devices. ASTM International 2010.

2. ASTM International. Standard Practice for Laboratory Immersion Corrosion Testing of Metal. ASTM International 2004.

3. Beyar R. Novel approaches to reduce stent stenosis. Annals of the NY Academy of Sciences 2004, 367-78.

4. Bennet MR. In-stent stenosis: pathology and implications for the development of drug eluting stents. Heart 2003, 89(2): 218-224.

5. Bosiers M. AMS INSIGHT: Absorbable metal stent implantation for treatment of below-the-knee critical limb ischemia: 6-month analysis. Cardiovasc Interv Radiol, 2009: 424-435.

6. Bouma BE. Evaluation of intracoronary stenting by intravascular optical coherence tomography. Heart 2003, 89: 317-320.

7. Brezinski M, Saunders K, Jesser C, Li X, Fujimoto J. Index matching to improve optical coherence tomography imaging through blood. Circulation 2001, 103: 1999-2003.

8. Brezinski M.E, Tearney G.J, Weissman N.J, Boppart S.A, Bouma B.E, Hee M.R, Weyman A.E, Swanson E.A, Southern J.F, Fujimoto J.G. Assessing atherosclerotic plaque morphology: comparison of optical coherence tomography and high frequency intravascular ultrasound. Heart 1997, 77: 397-403.

9. Brezinski M.E, Tearney GJ, Bouma B.E, Izatt J.A, Hee M.R, Swanson E.A, et al. Optical coherence tomography for optical biopsy. Properties and demonstration of vascular pathology. Circulation 1996, 93(6): 1206-1213.

10. Choy J.S, Mathieu-Costello O, Kassab G.S. The effect of fixation and histological preparation on coronary artery dimensions. Ann Biomed Eng 2005, 33(8): 1027-1033.

11. Colombo A, Hall P, Nakamura S, Almagor Y, Maiello L, Martini G, et al. Intracoronary stenting without anticoagulation accomplished with intravascular ultrasound guidance. Circulation 1995, 1891-1897.

12. Colombo A, Karvouni E. Biodegradable Stents: Fulfilling their mission and stepping away. Circulation 2000, 102: 371-373.

13. Craig P, Zak B, Iseri L.T, Boyle A.J, Myers G.B. Am J Clin Pathol. Nov 2, 1951.

14. Dagres N, Erbel R. Comparison between PTCA and bypass operation. Results of large randomized studies. Med Klin (Munich). 1998, 93(1): 22-26.

15. Dhein S, Mohr F, Delmar M. Classical histological staining procedures in cardiovascular research. Berlin Heidelberg Springer 2005, 485-499.

16. Di Mario C, Griffiths H, Goktekin O, Peeters N, Verbist J, Bosiers M, Deloose K, Heublein B, Rohde R, Kasese V, Ilsley C, Erbel R. Drug-eluting bioabsorbable magnesium stent. J Interv Cardio 2004, l391-1395.

17. Dobrin, P.B. Effect of histologic preparation on the cross sectional area of arterial rings. J Surg Res 1996, 61(2): 413-415.

18. Driesen, R.B, Zalewski J, Driessche N.V, Vermeulen K, Bogaert J, Sipido K.R, Van de Werf F, Claus P. Histological correlate of a cardiac magnetic resonance imaged microvascular obstruction in a porcine model of ischemia–reperfusion. Cardiovascular Pathology 2011, 21(3): 129-131.

19. D'Souza, S, Ferrante G, Tyczynski P, Di Mario C. Biodegradable stents – a new era? European Cardiology 2008, 4(2): 82-84.

20. Eagle, K.A, Guyton R.A, Davidoff R, Ewy G.A, Fonger J, Gardner T.J, Gott J.P, Herrmann H.C, Marlow R.A, Nugent W, O'Connor G.T, Orszulak T.A, Rieselbach R.E, Winters W.L, Yusuf S. ACC/AHA guidelines for coronary artery bypass graft surgery: executive summary and recommendations: a report of the American College of Cardiology/American Heart Association Task Force on Practice Guidelines. Circulation 1999, 1464-1480.

21. Erbel R, Ge J, Gorge G, Haude M. Intravascular ultrasound limitations and unresolved issues. The International Journal of Cardiac Imaging 1995, 11(1): 15-19.

22. Erbel R, Bose D, Haude M, et al. Absorbable coronary stents. New promising technology. Herz 2007, 308-319.

23. Erbel R, Di Mario C, Bartunek J, Bonnier J, de Bruyne B, Eberli F.R, Erne P, Haude M, Heublein B, Horrigan M. Temporary scaffolding of coronary arteries with bioabsorbable magnesium stents: a prospective, non-randomised multicentre trial. Lancet 2007, 369: 1869–1875.

24. Erne P, Schier M, Resink T.J. The road to bioabsorbable stents: reaching clinical reality? Cardiovasc Intervent Radiol 2006, 29(1): 11-16.

25. Ge J, Erbel R, Gerber T, et al. Intravascular ultrasound imaging of angiographically normal coronary arteries: a prospective study in vivo. Br Heart J 1994, 71(6): 572-578.

26. Ge J, Erbel R, Seidel I, et al. Experimental evaluation of the accuracy and safety of intraluminal ultrasound. Z Kardiol 1991, 80(10): 595-601.

27. Glick D, Freir E.F, Ochs M.J. Microdetermination of magnesium and its histological distribution in the adrenal in various functional states. J Biol Chem 1957, 226(77).

28. Gonzalo N, et al. Quantitative ex-vivo and in-vivo comparison of lumen dimensions measured by optical coherence tomography (OCT) and intravascular

ultrasound (IVUS) in human coronary arteries. Rev Esp Cardiol 2009, 62(6): 615-624.

29. Grube E, Gerckens U, Buellesfeld L, Fitzgerald P.J. Intracoronary imaging with optical coherence tomography: a new high-resolution technology providing striking visualization in the coronary artery. Circulation 2002, 106: 2409-2410.

30. Hall P, Nakamura S, Maiello L, Itoh A, Blengino S, Martini G, et al. A randomized comparison of combined ticlopidine and aspirin therapy versus aspirin therapy alone after successful intravascular ultrasound-guided stent implantation. Circulation 1996, 93: 215-222.

31. Hausmann D, Erbel R, Alibelli-Chemarin, M.J, et al. The safety of intracoronary ultrasound. A multicenter survey of 2207 examinations. Circulation 1995, 91(3): 623-630.

32. Hermanwan H, Dube D, Mantovani D. Developments in metallic biodegradable stents. Acta Biomaterialia. Oct 2009.

33. Heublein B, Rohde R, Kaese V, Niemeyer M, Hartung W, Haverich A, Biocorrosion of magnesium alloys: a new principle in cardiovascular implant technology? Heart 2003, 89: 651-656.

34. Hlatky M.A, Rogers W.J, Johnstone I, Boothroyd D, Brooks, Pitt B, Reeder G, Ryan T, Smith H, Whitlow P, Wiens R, Mark D.B, Rosen A.D, Detre K, Frye R.L. Medical care costs and quality of life after randomization to coronary angioplasty or coronary bypass surgery. N Engl J Med 1997, 336: 92-99.

35. Hofma S.H, van der Giessen W.J, van Dalen B.M, et al. Indication of long-term endothelial dysfunction after sirolimus eluting stent implantation. Eur Heart J 2006, 27: 166-170.

36. Holmes D.R Jr, Leon M.B, Moses J.W, Popma J.J, Cutlip D, Fitzgerald P.J, Brown C, Fishel T, Wong S.C, Midei M, Snead D, Kuntz, R.E. Analysis of 1-year clinical outcomes in the SIRIUS trial: a randomized trial of a sirolimus-eluting stent versus a standard stent in patients at high risk for coronary restenosis. Circulation 2004, 109(5): 634-640.

37. Huang D, Swanson E.A, Lin C.P, et al. Optical coherence tomography. Science 1991, 254: 1178-1781.

38. Huda H, Coltart J. Miracle stents - a future without restenosis. McGill Journal of Medicine, July 7, 2007: 105-111.

39. Jang I.K, Bouma B.E, Kang D.H, Park S.J, Park S.W, Seung K.B, et al. Visualization of coronary atherosclerotic plaques in patients using optical coherence tomography: comparison with intravascular ultrasound. J Am Coll Cardiol 2002, 604(39): 9-17.

40. Jang I.K, Tearney G, MacNeill B, Takano M, Moselewski F, Iftima N, Shishkov M, Houser S, Aretz H.T, Halpern E.F, Bouma, B.E. In vivo characterization of coronary atherosclerotic plaque by use of optical coherence tomography. Circulation 2005, 111: 1511-1555.

41. Joner M, Finn A.V, Farb A, et al. Pathology of drug eluting stents in humans: delayed healing and thrombotic risk. J Am Coll Cardiolpathology 2006, 48: 193-202.

42. Kataiwa H.A, Tanaka H.K, Imanishi T, Akasaka T. Safety and usefulness of non-occlusion image acquisition technique for optical coherence tomography. Circ J 2008, 72 (9): 1536-1537.

43. Kawase Y, et al. In vivo volumetric analysis of coronary stent using optical coherence tomography with a novel balloon occlusion-flushing catheter: a comparison with intravascular ultrasound. Ultrasound Med Biol October 2005, 31(10): 1343-1350.

44. Kolthoff I.M. Chem Week, 1927: 254 (24).

45. Kumar, G.L, Kiernan J.A, Pathology, education guide: special stains ans H & E. Carpinteria, California. Dako, 2010.

46. Kume T, et al. Assessment of coronary intima-media thickness by optical coherence tomography: comparison with intravascular ultrasound. Circ J 2005, 69: 903-907.

47. Leber A.W, Knez A, Becker A, et al. Accuracy of multidetector spiral computed tomography in identifying and differentiating the composition of coronary atherosclerotic plaques: a comparative study with intracoronary ultrasound. J Am Coll Cardiol 2004, 43 (7): 1241-1247

48. Matsumoto D, et al. Neointimal coverage of sirolimus-eluting stents at 6-month follow-up: evaluated by optical coherence tomography. Eur Heart J 2007, 28 (8): 961-967.

49. Mintz G.S, et al. American college of cardiology clinical expert consensus document on standards for acquisition, measurement and reporting of intravascular ultrasound studies (IVUS). Am Coll of Cardiology 2001.

50. Morice M.C, Zemour G, Beneviste E, Biron Y, Bourdonnec C, Faivre R, et al Intracoronary stenting without coumadin: one month results of a French multicenter study. Cathet Cardiovasc Diag 1995, 35: 1-7.

51. Movat H.Z, Demonstration of all connective tissue elements in a single section; pentachrome stains. AMA Arch Pathol Sept 1955, 60(3): 289-295.

52. Murabito, J.M, Evans, J.C, Larson M.G, Levy D. Prognosis after the onset of coronary heart disease: an investigation of differences in outcome between the sexes according to initial coronary disease presentation. Circulation 1993, 295: 2482.

53. Murray C.J, Lopez A.D. Alternative projections of mortality and disability by cause 1990–2020: Global Burden of Disease Study. Lancet 1997, 349: 1498-1504.

54. Müller W, Firsching R. Demonstration of elastic fibers with reagents for detection of magnesium. J Anat 1991, 175: 195-202.

55. Nebeker J.R, Virmani R, Bennet C.L, et al. Hypersensitivity cases associated with

drug eluting coronary stents: a review of available cases from the research on adverse drug events and reports (RADAR) project. J Am Coll Cardiol 2006, 47: 175-181.

56. Nissen S.E, Yock P. Intravascular ultrasound: novel pathophysiological insights and current clinical applications. Circulation 2001, 103(4): 604-616.

57. Pasterkamp G, Falk E, Woutman H, Borst C. Techniques characterizing the coronary atherosclerotic plaque: influence on clinical decision making? Am Coll Cardiol J 2000, 36(1): 13-21.

58. Patwari P, Weissman N.J, Boppart S.A, et al. Assesment of coronary plaque with optical coherence tomography and high frequency ultrasound. Am J Cardiol 2000, 85(5): 641-644.

59. Peeters P, Bosiers M, Verbist J, Deloose K, Heublein B. Preliminary results after application of absorbable metal stents in patients with critical limb ischemia. J Endovasc Ther 2005, 12(1): 1-5.

60. Peuster M, Wohlsein P, Brugmann M, Ehlerding M, Seidler K, Fink C, et al. A novel approach to temporary stenting: degradable cardiovascular stents produced from corrodible metal – results 6-18 months after implantation into New Zealand white rabbits. Heart 2001, 86: 563-569.

61. Pinto T, Slottow T.L, Pakala R, Waksman R. Serial imaging and histology illustrating the degradation of a bioabsorbable magnesium stent in a porcine coronary artery. Eur Heart J 2008, 29(3): 314.

62. Pinto, T, Waksman R. Clinical applications of optical coherence tomography. J Interv Cardiol 2006, 19(6): 566-573.

63. Prati F, Pawlowski T, Sommariva L, Labellarte A, Manzoli A, Boccanelli A, et al. Intravascular ultrasound and quantitative coronary angiography assessment of late in-stent restenosis: in vivo human correlation and methodological implications. Catheter Cardiovasc Interv 2002, 57 (2): 155-160.

64. Ratner, B.D, Biomaterials Science: An Introduction to Materials in Medicine. Academic Press, San Diego, 1996.

65. Regar E, Werner F, Klauss V, et al. IVUS analysis of the acute and long-term stent result using motorized pullback: intraobserver and interobserver variability. Catheter Cardiovasc Interv 1999, 48(3): 245-250.

66. Russell, H.K Jr. A Modification of Movat's Pentachrome Stain. Arch Pathol 1972, 94(2): 187-191.

67. Saroj S.J, Todd G, Joseph F.T Jr. The Movat Pentachrome Stain as a means of identifying microcrystalline cellulose among other particulates found in lung tissue. Archives of Pathology and Laboratory Medicine 2011, 135(2).

68. Serruys, P.W, Ormiston J.A, Onuma Y, Regar E, Gonzalo N, Garcia H.M. A bioabsorbable everolimus-eluting Coronary Stent System (ABSORB): 2-year outcomes and results from multiple imaging methods. The Lancet 2009, 373(9667): 897-910.

69. Siegel R.J, Swan K, Edwalds G, Fishbein M.C. Limitations of postmortem assessment of human coronary artery size and luminal narrowing: differential effects of tissue fixation and processing on vessels with different degrees of atherosclerosis. J Am Coll Cardiol 1985, 5: 342-346.

70. Sigma-Aldrich. Thiazole Yellow G for microscopy (fluorescence indicator), adsorption indicator, www.sigmaaldrich.com/catalog/product/fluka/88390.

71. Striowsky E, Minischweine. Kosmos Verlag, Stuttgart, 2006.

72. Suzuki Y, Ikeno F, Koizumi T, Tio F, Yeung A.C, Yock P.G, et al. In vivo comparison between optical coherence tomography and intravascular ultrasound for detecting small degrees of in-stent neointima after stent implantation. J Am Coll Cardiol Intv 2008, 1: 168-173.

73. Sigwart U, Puel J, Mirkovitch V, Joffre F. Intravascular stents to prevent occlusion and restenosis after transluminal angioplasty. N Engl J Med 1987, 316(12): 701-706. .

74. St. Goar F, Pinto F, Alderman E, et al. Detection of coronary atherosclerosis in young adult hearts using intravascular ultrasound. Circulation 1992, 86(3): 756-763.

75. Stack R, Califf R, Phillips H, et al. Interventional cardiac catheterization at Duke Medical Center. Am J Cardiol 1988, 62: 3F-24F.

76. Takano M, et al. Long-term follow-up evaluation after sirolimus-eluting stent implantation by optical coherence tomography: do uncovered struts persist? J Am Coll Cardiol 2008, 51(9): 968-969.

77. Tanigawa J, et al. Optical coherence tomography to assess malapposition in overlapping drug-eluting stents. Euro Interv 2008, 3: 580-583.

78. Tanimoto S, et al. A novel approach for quantitative analysis of intracoronary optical coherence tomography: high inter-observer agreement with computer-assisted contour detection. Catheter Cardiovasc Interv 2008, 72(2): 228-235.

79. van der Giessen W, Lincoff M, Schwartz R.E. Marked inflammatory sequelae to implantation of biodegradable and nonbiodegradable polymers in porcine coronary arteries. Circulation 1996, 94: 1690-1697.

80. Waksman R, Pakala R, Kuchulakanti P, Baffour R, Hellinga D, Seabron R, et al. Safety and efficacy of bioabsorbable magnesium alloy stents in porcine coronary arteries. Cardiovasc Interv Catheter 2006, 68: 607-617.

81. Yabushita H, Bouma B, Houser S, Aretz H, Jang I, Schlendorf K, et al. Characterization of human atherosclerosis by optical coherence tomography. Circulation 2002, 106: 1640-1645.

82. Yamaguchi T, et al. Safety and feasibility of an intravascular optical coherence tomography image wire system in the clinical setting. Am J Cardiol 2008, 101(5): 562-567.

83. Yang X, Manninen H, Matsi P, Soimakallio S. Percutaneous endovascular

stenting: development, investigation and application. Eur J Radiol 1991, 13(3): 161-173.

84. Zimarino M, et al. Optical coherence tomography accurately identifies intermediate atherosclerotic lesions – An in vivo evaluation in the rabbit carotid artery. Atherosclerosis 2007, 193(1): 94-101.

Abbreviations

AMS: Absorbable Metal Stent

ASTM: American Society for Testing and Materials

BMS: Bare Metal Stent

CABG: Coronary Artery Bypass Graft

CAD: Coronary Artery Disease

CT: Computed Tomography

DES: Drug Eluting Stent

DICOM: Digital Imaging and Communications in Medicine

DREAMS: Drug Eluting Absorbable Metal Scaffold

EEL: External Elastic Lamina

HU: Hounsfield Units

IEL: Internal Elastic Lamina

IVUS: Intravascular Ultrasound

LAD: Left Anterior Descending

LCx: Left Circumflex

MPS: Movat's Pentachrome Staining

MRI: Magnetic Resonance Imaging

NURD: Non-Uniform Rotational Distortion

OCT: Optical Coherence Tomography

PCI: Percutaneous Coronary Intervention

PLLA: Polymer of Poly-L-Lactide

PTCA: Percutaneous Transluminal Coronary Angioplasty

RCA: Right Coronary Artery

SD: Standard Deviation

TVR: Target Vessel Revascularization

2D: Two-Dimensional

Acknowledgements

There are many people who selflessly gave their time, talents, and support to assist me throughout my medicine degree. It is a pleasure to thank them for making this thesis possible.

First and foremost, I'd like to express my deepest gratitude to Raphael Weiner, the most supportive and patient person I have ever known! Thank you for being with me and motivating me throughout this journey. His editing suggestions and precise sense of language contributed to the thesis. Without his encouragement and understanding it would have been impossible for me to finish this work.

To Professor Volker Klaus, M.D. I owe a sincere thank you for giving me the chance to work under his supervision at the Institute of Interventional Cardiology of LMU.

I am deeply grateful to my supervisor, Dr. Johannes Rieber, M.D. His extensive knowledge, enthusiasm for this work, and support has been invaluable. Thank you for your guidance and patience over the last couple years.

To Dr. E. Wittchow from Biotronik, thank you for the great cooperation.

I extend my thanks to Professor Andreas Schober, M.D. for providing a great work environment in his lab and his stimulating ideas about the Titan-Yellow stain.

I am in a great debt to Andrea Millet, who patiently taught me how to stain, how to use different kinds of microscopes, and who spent long hours in lab with me to investigate different histological methods.

The team Interventional Cardiology team at LMU, thank you for all your help with my research.

Holger Hetterich, M.D. without your help, it would have been near impossible to get through the data collection phase. Thank you for sharing your experience and for taking valuable time out of your schedule to oversee my research.

To the Department of Pathology at LMU, for providing me access to their microscopes. I want to also use this opportunity to thank Prof. Weiss, M.D. for

answering my specific questions about the vessel histopathology.

I would like to dedicate this work to my loving parents Nurgül and Süleyman, to my dear sister Burçin, and my caring grandmother Mükü. Thank you for your endless love, generosity, support, and for instilling in me the value of hard work and respect.

Eidesstattliche Erklärung

Hiermit erkläre ich, dass ich die vorliegende Arbeit eigenständig und ohne fremde Hilfe angefertigt habe. Textpassagen, die wörtlich oder dem Sinn nach auf Publikationen oder Vorträgen anderer Autoren beruhen, sind als solche kenntlich gemacht.
Die Arbeit wurde bisher keiner anderen Prüfungsbehörde vorgelegt und auch noch nicht veröffentlicht.

München, den 11.04.2014 Burcu Gül